

POLITECNICO DI TORINO

Dipartimento di Ingegneria Meccanica e
Aerospaziale
Corso di Laurea in Ingegneria Aerospaziale

Tesi di Laurea

**Investigation on the effects of the
planetary radiation pressure on
solar sails**



Relatori:

Dr. Matteo Ceriotti

Prof. Lorenzo Casalino

Candidata:

Alessia De Iuliis

Marzo 2019

A Domenico.

Acknowledgments

Vorrei ringraziare il professor Matteo Ceriotti per aver creduto in me ed avermi dato la possibilità di svolgere questo lavoro di tesi. Un grazie va anche al professor Lorenzo Casalino per i preziosi consigli e la disponibilità.

Grazie alla mia grande famiglia. Ovunque io sia nel mondo, riuscite sempre a farmi sentire il vostro amore e il vostro sostegno. Ed infine, grazie ai miei amici, persone preziose che hanno reso questi anni speciali.

Table of contents

Acknowledgments	ii
1 Introduction	1
1.1 History of solar sailing	2
1.2 Planetary solar sailing	2
1.3 Planetary radiation pressure	4
1.4 Aims of the work	4
2 Models	6
2.1 Solar radiation pressure	8
2.1.1 Quantum description	8
2.1.2 Solar sail as a perfect reflector	10
2.1.3 Optical force model	11
2.2 Planetary radiation pressure	13
2.2.1 Black body radiation pressure	16
2.2.2 Albedo	17
3 Methodology	20
3.1 Analytical law	20
3.2 Numerical approach	25
4 Results	27
4.1 Maximum magnitude of the acceleration	27
4.1.1 SRP	27
4.1.2 SRP+BBRP	30
4.2 Maximum radial acceleration	34
4.2.1 SRP	35
4.2.2 SRP+BBRP	37
4.2.3 SRP+ARP	40
4.2.4 SRP+PRP	42
4.3 Maximum transversal acceleration	47

4.3.1	SRP	47
4.3.2	SRP+BBRP	48
4.3.3	SRP+ARP	51
4.3.4	SRP+PRP	53
5	Control law for semi-major axis increase	59
5.1	Earth	61
5.2	Venus	72
6	Conclusions	81
A	Eletromagnetic description	83
	Bibliography	85

List of figures

2.1	Reference frame for a sail orbiting around a planet.	7
2.2	Cylindrical eclipse model.	8
2.3	Incident photons direction and reflected photons direction.	11
2.4	Radiation specific intensity.	14
2.5	Planetary radiation pressure with a finite angular sized disc.	15
2.6	Planet heating geometry for a view factor calculation: on the left one side is heated, on the right both sides are heated.	18
2.7	Reflection angle.	18
3.1	Reference frame with angles.	21
3.2	Behaviour of the transversal acceleration in different points around the planet	24
4.1	Maximisation of the magnitude of the acceleration, for a single-side coating sail around the Earth subject to SRP.	28
4.2	Maximisation of the magnitude of the acceleration, for a single-side coating sail around Mercury subject to SRP.	29
4.3	Maximisation of the magnitude of the acceleration, for a single-side coating sail around Mars subject to SRP.	29
4.4	Maximisation of the magnitude of the acceleration, for a single-side coating sail around Venus subject to SRP.	30
4.5	Maximisation of the magnitude of the acceleration, for a single-side coating sail around the Earth subject to SRP and BBRP.	31
4.6	Maximisation of the magnitude of the acceleration, for a double-side coating sail around the Earth subject to SRP and BBRP.	31
4.7	Maximisation of the magnitude of the acceleration, for a single-side coating sail around Mercury subject to SRP and BBRP.	32
4.8	Maximisation of the magnitude of the acceleration, for a single-side coating sail around Mars subject to SRP and BBRP.	33
4.9	Maximisation of the magnitude of the acceleration, for a single-side coating sail around Venus subject to SRP and BBRP.	34

4.10	Maximisation of the magnitude of the acceleration, for a double-side coating sail around Venus subject to SRP and BBRP.	34
4.11	Maximisation of radial acceleration, for a single-side coating sail around Earth subject to SRP.	35
4.12	Maximisation of radial acceleration, for a single-side coating sail around Venus subject to SRP.	36
4.13	Maximisation of radial acceleration, for a single-side coating sail around Earth subject to SRP and BBRP.	37
4.14	Maximisation of radial acceleration, for a double-side coating sail around Earth subject to SRP and BBRP.	38
4.15	Maximisation of radial acceleration, for a single-side coating sail around Venus subject to SRP and BBRP.	39
4.16	Maximisation of radial acceleration, for a double-side coating sail around Venus subject to SRP and BBRP.	40
4.17	Maximisation of radial acceleration, for a single-side coating sail around Earth subject to SRP and ARP.	41
4.18	Maximisation of radial acceleration, for a double-side coating sail around Earth subject to SRP and ARP.	41
4.19	Maximisation of radial acceleration, for a single-side coating sail around Venus subject to SRP and ARP.	42
4.20	Maximisation of radial acceleration, for a double-side coating sail around Venus subject to SRP and ARP.	42
4.21	Maximisation of radial acceleration, for a single-side coating sail around Earth subject to SRP and PRP.	43
4.22	Maximisation of radial acceleration, for a double-side coating sail around Earth subject to SRP and PRP.	44
4.23	Maximisation of radial acceleration, for a single-side coating sail around Venus subject to SRP and PRP.	45
4.24	Maximisation of radial acceleration, for a double-side coating sail around Venus subject to SRP and PRP.	46
4.25	Maximisation of transversal acceleration, for a single-side coating sail around Earth subject to SRP.	48
4.26	Maximisation of transversal acceleration, for a single-side coating sail around Venus subject to SRP.	48
4.27	Maximisation of transversal acceleration, for a single-side coating sail around Earth subject to SRP and BBRP.	49
4.28	Maximisation of transversal acceleration, for a double-side coating sail around Earth subject to SRP and BBRP.	50
4.29	Maximisation of transversal acceleration, for a single-side coating sail around Venus subject to SRP and BBRP.	51

4.30	Maximisation of transversal acceleration, for a double-side coating sail around Venus subject to SRP and BBRP.	51
4.31	Maximisation of transversal acceleration, for a single-side coating sail around Earth subject to SRP and ARP.	52
4.32	Maximisation of transversal acceleration, for a double-side coating sail around Venus subject to SRP and ARP.	52
4.33	Maximisation of transversal acceleration, for a single-side coating sail around Venus subject to SRP and ARP.	53
4.34	Maximisation of transversal acceleration, for a double-side coating sail around Venus subject to SRP and ARP.	53
4.35	Maximisation of transversal acceleration, for a single-side coating sail around Earth subject to SRP and PRP.	54
4.36	Maximisation of transversal acceleration, for a double-side coating sail around Earth subject to SRP and PRP.	55
4.37	Maximisation of transversal acceleration, for a single-side coating sail around Venus subject to SRP and PRP.	56
4.38	Maximisation of transversal acceleration, for a double-side coating sail around Venus subject to SRP and PRP.	57
5.1	Control law	61
5.2	Trajectory around the Earth with orientation of the sail with $\omega = 0$ deg	62
5.3	Results for a sail around the Earth with $\omega = 0$ deg.	63
5.6	Results for a sail around the Earth with $\omega = 90$ deg.	66
5.7	Trajectory around the Earth with orientation of the sail with $\omega = 180$ deg.	67
5.8	Results for a sail around the Earth with $\omega = 180$ deg.	68
5.9	Trajectory around the Earth with orientation of the sail with $\omega = 270$ deg.	69
5.10	Results for a sail around the Earth with $\omega = 270$ deg.	70
5.11	Trajectory around Venus with orientation of the sail with $\omega = 0$ deg .	72
5.12	Results for a sail around Venus with $\omega = 0$ deg.	73
5.13	Trajectory around Venus with orientation of the sail with $\omega = 90$ deg	74
5.14	Results for a sail around Venus with $\omega = 90$ deg.	75
5.15	Trajectory around Venus with orientation of the sail with $\omega = 180$ deg	76
5.16	Results for a sail around Venus with $\omega = 180$ deg.	77
5.17	Trajectory around Venus with orientation of the sail with $\omega = 270$ deg	78
5.18	Results for a sail around Venus with $\omega = 270$ deg.	79

List of tables

3.1	Solar radiation pressure at the mean distance between the Sun and the planet, specific characteristic acceleration, planet radius, planet mean temperature, luminosity due to the BBRP and solar flux in orbit for different planets.	26
3.2	Value of the reflection and absorption coefficients for the back- and front-side of a single- and double-side reflective coating sail.	26
4.1	Value of the ratio $a_{SRP}/a_{0,s}$, $a_{SRP+BBRP}/a_{0,s}$ and corresponding percentage increase.	34
4.2	Value of the ratio of the maximum radial acceleration to the characteristic acceleration and the attitude angle σ that maximises the acceleration in the cases SRP and SRP+PRP for a sail in the vicinity of the Earth.	44
4.3	Value of the ratio of the maximum radial acceleration to the characteristic acceleration and the attitude angle σ that maximises the acceleration in the cases SRP and SRP+PRP for a sail in the vicinity of Venus.	46
4.4	Value of the ratio of the maximum transversal acceleration to the characteristic acceleration and the attitude angle σ that maximises the acceleration in the cases SRP and SRP+PRP for a sail in the vicinity of the Earth.	55
4.5	Value of the ratio of the maximum transversal acceleration to the characteristic acceleration and the attitude angle σ that maximises the acceleration in the cases SRP and SRP+PRP for a sail in the vicinity of Venus.	57
5.1	Orbital elements	60
5.2	Value of the percentage increase of the semi-major axis considering SRP only, SRP+PRP and the corresponding absolute percentage increase for a sail orbiting around the Earth.	71

5.3	Value of the percentage increase of the semi-major axis considering SRP only, SRP+PRP and the corresponding absolute percentage increase for a sail orbiting around Venus.	80
5.4	Orbital element at the initial and final time for different trajectories around Earth and Venus.	80

Nomenclature

ARP Albedo Radiation Pressure

BBRP Black-Body Radiation Pressure

GTO Geosynchronous Transfer Orbit

PRP Planetary Radiation Pressure

PRP Solar Radiation Pressure

U3P Union pour la Promotion de la Propulsion Photonique

WSF Word Space Foundation

Chapter 1

Introduction

Solar sailing has for many years been an intriguing concept for spacecraft propulsion. A solar sail is a huge, ultra-thin reflective membrane unfurling in space. It is a unique form of propulsion which transcends reliance on reaction mass. In fact, solar sail gains momentum from an ambient source, the photon radiation pressure. Using a quantum description of radiation as packets of energy, photons can be visualized as travelling radially outwards from the body and scattering off the sail thus imparting momentum. Since solar sails are not limited by a finite reaction mass, they can provide continuous, albeit small, acceleration. The only limitation is the lifetime of the sail film due to the space environment.

The momentum carried by individual photons is extremely small, at best a solar sail will experience $9 \cdot 10^{-6}$ N of force per square metre of sail located in Earth orbit [1]. In order to intercept large number of photons, the sail should have a large surface. However, it should also maintain the lowest possible mass to generate the highest acceleration from the momentum transported by photons. Adding the impulse due to incident and reflected photons, the ideal thrust vector is found to be directed approximately normal to the surface of the sail. Hence, it is possible to gain or reduce the orbital angular momentum controlling the orientation of the sail relative to the Sun. Thanks to this, solar sails can be used in a wide range of missions such as lunar fly-by's [5], [6], inner [7] and outer [8] solar system rendezvous missions and could offer potential low-cost operations [9] and flexible manoeuvres for exploring the solar system [10].

The orbital dynamics of solar sail uses a small continuous thrust to modify the orbit over an extended period of time, this concept is similar to the electric low thrust propulsion system dynamics, and it can be used, for example, in deep space interplanetary or Lagrange point missions or celestial body-bounded orbit. Some possible applications for the latter are heliocentric and planetary orbits.

1.1 History of solar sailing

Solar sailing has caught the interest of many since its introduction during the beginning of the 1900s. The concept of solar sailing dates back to the 1920s in the work of Konstantin Tsiolkovsky, Soviet father of astronautics, and Fridrick Tsander, his co-worker. After their idea of "using tremendous mirrors of very thin sheets" and "using the pressure of sunlight to attain cosmic velocities" [1], a dormant period of over thirty years followed. During the late 1950s and early 1960s the concept of solar sailing received renewed interest, with studies aiming to explore the problem and benefits of this novel concept. However, it was just in the 1970s that the first major mission design study of the concept was developed for a proposed Halley's comet rendezvous mission. In the end this mission was dropped, but the interest in solar sailing was still high. Word Space Foundation (WSF) tried to continue to develop solar sail and to achieve a small-scale demonstration flight. Moreover to promote solar sail technology, the idea of an ambitious race to the Moon was proposed by the Union pour la Promotion de la Propulsion Photonique (U3P) in 1982. However it is just in the last three decades that, thanks to the advances in microelectronics, carbon fibre booms and thin film manufacturing, solar sail has become a technology applicable in real missions [2], as can be seen from NASA's Nanosails-D2 [3]. It is a large, low-mass high-surface-area sail, deorbiting from the upper layers of the atmosphere. This device proved the deorbiting capabilities of a sail and the possibility of deploying a sail in atmosphere. Another demonstrator is CubeSail [4], it is a nano-solar sail, inserted in a Sun-synchronous orbit, designed by Surrey Space Centre, University of Surrey. The primary aim of the mission is to demonstrate the concept of solar sailing and the use of the sail membrane as a drag-sail to perform an end-of-life de-orbiting. The actual demonstration of the feasibility of solar sailing, came in 2010, when the Japan Aerospace Exploration Agency's spacecraft IKAROS successfully deployed the first solar sail in space.

1.2 Planetary solar sailing

In the work of Macdonald and McInnes [11], some potential solar sails applications are presented. Two highly significant planet-centred solar sail concepts are the GeoSail [12] and the Mercury Sun-Synchronous Orbiter [13]. These two solar sail mission concepts are very similar, since both use a solar sail to independently vary a single orbit parameter. The GeoSail mission concept aims in achieving long stay times in Earth's magnetotail, enabling a nominal duration of two years. The study was conducted for three kind of propulsion system: solar sailing, electric and chemical propulsion. In the end the reduction in launch mass and cost decreed

solar sail as the optimal propulsion system and it was found that the mission concept provided an excellent solar sail technology demonstration option. The mission MESSAGE (MErcury Solar Sail Advanced Geoscience Exploration)[13] proposed a solar sail spacecraft delivering a limited but highly valuable science payload to a Sun-synchronous Mercury orbit for three and a half years. The sail is used as a transportation means for the interplanetary transfer, for orbit capture upon Mercury arrival, and subsequent adjustment of a Sun-synchronous orbit about the planet near the terminator. In this case the vicinity of the Sun makes solar sailing very effective and the reduction of the launch mass enable the use of relative low-cost launch vehicles.

Another important application of solar sailing in planet-centred trajectory is the use of the sail to perform an escape manoeuvre. Coverstone and Prussing [14] developed a technique for escaping the Earth using a solar sail with a spacecraft initially in a geosynchronous transfer orbit (GTO) . The approach maximizes the instantaneous rate of increase of the total orbital energy, continuously orienting the sail in three dimensions to maximize the component of the sail force along the velocity vector. This strategy does not lead to a minimum-time solution, but if the characteristic acceleration of the sail has a magnitude of 1 mm/s^2 then this method leads to a near-minimum-time solution [15]. A more accurate study on Earth escape strategies has been conducted by Macdonald and McInnes [16], using blending locally optimal control law. These blended-sail control algorithms, explicitly independent of time, provides a near-optimal escape trajectories and maintains a safe minimum altitude. A range of initial conditions is analysed, maintaining the optimality by using a single-energy gain control law but without the risk of planetary collision. When the sail is in atmosphere, aerodynamic forces are exerted on the sail too. Stolbunov et al. [17] developed a dynamic model of the sail in three-dimension (3-D) and the expressions for the acceleration due to both solar radiation pressure and aerodynamic forces. Moreover they express the variation of the inclination and of the semimajor axis as a function of the attitude of the sail, showing the change of inclination that a spacecraft can potentially achieve in a year long mission, starting from a circular orbit with different altitude and characteristic accelerations. Mengali and Quarta [18] also analysed the effect of aerodynamic drag on solar sail trajectories. In this work the sail is treated as a flat plate and a hyperthermal flow model is assumed. Results show that near-minimum time trajectories for low characteristic acceleration are obtained. The steering law is shown to depend on the ratio between the local dynamic pressure and the solar radiation pressure on the sail.

1.3 Planetary radiation pressure

Different studies for a sail orbiting around a planet have been showed, all the cases however were not considering that a planet is a body that emits radiations and reflects part of the radiations coming from the Sun.

The planet, being a body in thermodynamic equilibrium with its environment, emits the so called Black-Body Radiation. This radiation is emitted uniformly in all direction, with most of the energy emitted in the infrared range. The specific spectrum and intensity of this radiation depends only on the body temperature. Moreover the radiation coming from the Sun will hit the planet and it will be reflected diffusely from the planet surface into the outer space as a function of the position of the Sun. This radiation is known as Albedo and it varies with geological and environmental features. The sum of the Black-Body Radiation Pressure and the albedo will be called Planetary Radiation Pressure. These photons will also hit the sail film, affecting the sail acceleration and thus changing its dynamics.

The contribution of the Albedo Radiation Pressure has been studied in the literature in the work of Grøtte and Holzinger [19]. The authors have studied the combined effects of SRP and Albedo Radiation Pressure in the circular restricted three body problem, for a system consists of Sun, a reflective minor body and the solar sail. The results show the presence of additional artificial equilibrium points in the volume between L_1 and L_2 points. In the work the reflective minor body considered could be any body with discernible albedo such as Earth, Mars or an asteroid.

1.4 Aims of the work

The contribution of the PRP has never been fully considered, hence in this work the combined effect of both solar and planetary pressures on a sail orbiting around a planet is studied. The first part of the work focused on finding the optimal attitude that maximises the acceleration along a given direction considering SRP and PRP . At first orbits around Mercury, Venus, Earth and Mars have been considered. This showed that the most promising results have been obtained around Earth and Venus. We studied these combined effects around a planet for two type of sail: single- and double-side reflective coating. Results show potential increase in the net acceleration and a change in optimal attitude to maximise the acceleration in a given direction. To conclude the study an optimal semi-major axis increase trajectory is shown with and without the PRP, to quantify the difference on a real-case scenario.

In the next chapter the mathematical model is presented, together with SRP and PRP force models and their resulting accelerations. The study proceeds with the explanation of the used methodology in chapter three.

Results for different planets considering different contributions (solar, black-body

and albedo) are shown in chapter four. In chapter five trajectories for increasing the orbital energy of a sail around a planet are shown. Finally conclusions are presented in chapter six.

Chapter 2

Models

This work aims to study the behaviour of a solar sail orbiting around a planet, subject to SRP and PRP. A two dimensional two-body problem is used to simplify the analysed situation, considering the sail in the ecliptic plane. The reference frame is centred in the planet, as can be seen in Fig. 2.1. Along the x -axis at a distance of R_{S-P} from the origin, lies the Sun, considered fixed. The y -axis is normal to x in the ecliptic plane. The distance between the sail and the origin is $r = \sqrt{x^2 + y^2}$ and the angle between r and x -axis is called θ .

The configuration used for the study is a flat solar sail. It is possible to define the vector $\hat{\mathbf{n}}$

$$\hat{\mathbf{n}} = [\cos \sigma, \sin \sigma] \quad (2.1)$$

as the unit vector normal to the sail surface and $\hat{\mathbf{t}}$ as the transverse unit vector normal to $\hat{\mathbf{n}}$ with components

$$\hat{\mathbf{t}} = [-\sin \sigma, \cos \sigma] \quad (2.2)$$

Where σ is the angle that expresses the attitude of the sail. It is defined as the angle between $\hat{\mathbf{n}}$ and the positive x -axis and it is measured counter-clockwise between 0 and 2π . The second angle used for the attitude is λ , measured from $\hat{\mathbf{n}}$ to the y -axis. The latter is used in the case of a double-reflective coated sail and due to the symmetry of the problem, it lies between 0 and π .

In order to assess solar sail performance, a standard performance metric is introduced. The solar sail characteristic acceleration is the most common metric. It is defined as the solar radiation pressure acceleration experienced by a solar sail facing the Sun at a distance of one astronomical unit.

$$a_0 = (2\tilde{r} + \tilde{a}) \frac{P_{SRP}}{\sigma^*} \quad (2.3)$$

where $P_{SRP} = 4.56 \cdot 10^{-6} \text{ Nm}^{-2}$ [1] is the SRP, A is the sail surface, m is the sail mass and σ^* is the sail loading, where the dash is used to avoid confusion with the

attitude angle σ and it is expressed as the sail mass per unit area $\sigma^* = \frac{m}{A}$. The factor 2 added in Eq. 2.3 considers that the photons that hit the sail film are reflected, doubling the pressure exerted on the sail. Finally, a reflection (\tilde{r}) and absorption (\tilde{a}) coefficient are introduced to consider the optical characteristics of the sail. Since the sail is facing the Sun with the front side $\tilde{r} = 0.9$ and $\tilde{a} = 0.1$, as is explained in detailed in Section 2.1.3.

Since the study is conducted for different planets, we defined a specific characteristic acceleration, which is the acceleration experienced by a sail facing the Sun at a distance equal to the mean distance between the planet and the Sun, with the value of the pressure at that distance for that planet.

This study considers the combined effect of both SRP and PRP. With reference to Fig. 2.1, the photons emitted by the Sun generate a force exerted along the vector $\hat{\mathbf{u}}_i$, instead the $\hat{\mathbf{r}}$ shows the direction of the planetary radiation, radial from the planet. The angle between $\hat{\mathbf{n}}$ and $\hat{\mathbf{u}}_i$ is the pitch angle (α) and the angle between $\hat{\mathbf{n}}$ and $\hat{\mathbf{r}}$ is δ . These two angles can have values between $[0, \pi]$ to consider if the radiation is exerted on the front or on the back of the sail.

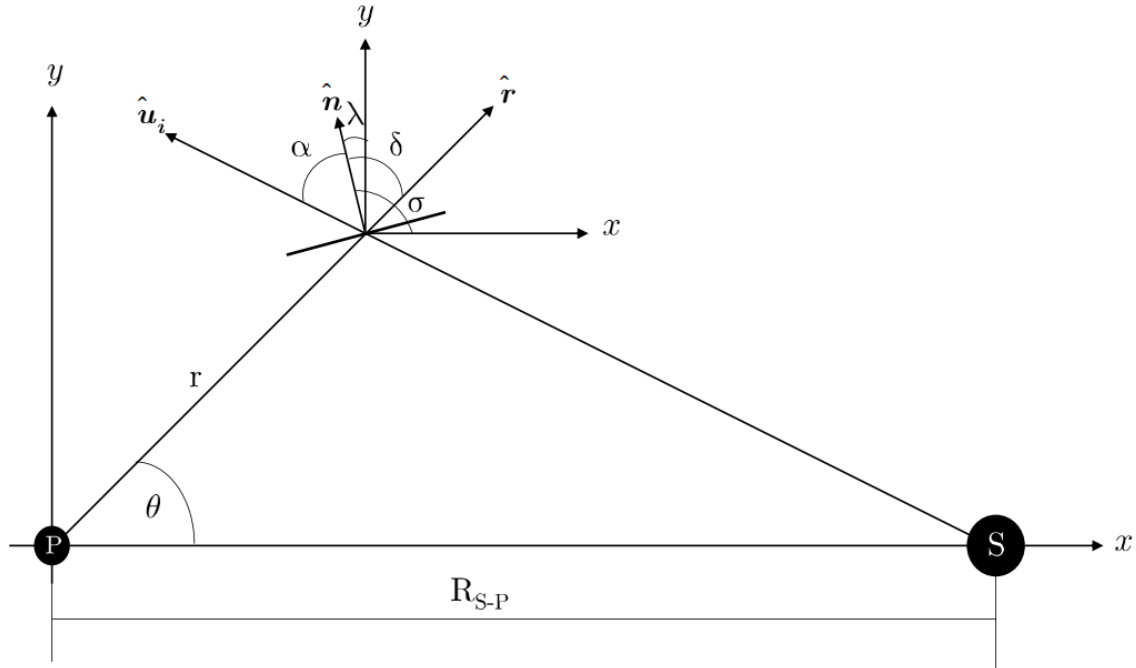


Figure 2.1: Reference frame for a sail orbiting around a planet.

It has been decided to consider also the presence of an umbra region in which the sail is in eclipse. In this zone the only contribution exerted on the sail is the PRP force. The eclipse has been modelled using a cylindrical eclipse model. In this

case the Sun is assumed to be infinitely far away from the planet, the divergence of the rays is small so the light rays can be considered as parallel, without making a consistent difference. This produces a cylindrical planet shadow with a radius equal to the planet radius (Fig. 2.2).

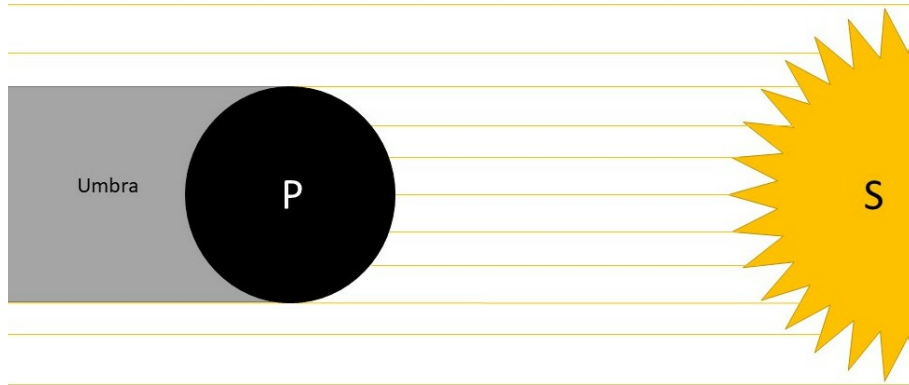


Figure 2.2: Cylindrical eclipse model.

2.1 Solar radiation pressure

Solar sailing is based on the force generated by the momentum transported to the sail by radiative energy from the Sun. The experimental verification of the existence of radiation pressure was performed in 1900 at the University of Moscow by Peter Lebedew. He finally succeeded in isolating radiation pressure using a series of elegant torsion balance experiments [1]. The physics of radiation pressure can be explained through two descriptions: quantum description and electromagnetic description. Since both of them lead to the same results, in the following section the quantum description is presented. The electromagnetic description is inserted in appendix A.

2.1.1 Quantum description

Using quantum mechanics, photons are the quantum packets of energy which make radiation. These photons transport a certain amount of momentum that is exerted on the sail and generates the radiation pressure.

It is possible to derive the value of the pressure using the derivation by McInnes [1].

Using Planck's law, it is possible to express the energy E transported by a photon of frequency ν as

$$E = \nu \bar{h} \quad (2.4)$$

where \bar{h} is Planck's constant. In addition to this quantum view, using the mass-energy equivalence of special relativity, the total energy of a moving body can be written as

$$E^2 = m_0^2 c^4 + p^2 c^2 \quad (2.5)$$

where m_0 is the rest mass of the body, p is its momentum and c is the speed of light. The equation shows the rest energy of the body in the first term and the energy due to its motion in the second term. Since a photon has zero mass at rest, its energy can be written as

$$E = pc \quad (2.6)$$

Equating Eqs. 2.4 and 2.6 it is possible to find the momentum transported by a single photon

$$p = \frac{\bar{h}\nu}{c} \quad (2.7)$$

In order to calculate the pressure exerted on a body, a flux of photons and their momentum must be considered. If you imagine surrounding the Sun with a series of imaginary spheres, the energy crossing the surface of each sphere is the same, irrespective of the radius of the sphere. For this reason the energy crossing unit area in unit time W at a distance r from the Sun may be written in terms of solar luminosity L_S and scaled by the Sun-Earth distance R_{S-E} , since $W4\pi r^2 = W_E 4\pi R_{S-E}^2$.

$$W = W_E \left(\frac{R_{S-E}}{r} \right)^2 \quad (2.8)$$

where W_E is the energy flux measured at the Earth's distance from the Sun and it can be calculated as

$$W_E = \frac{L_S}{4\pi R_E^2} \quad (2.9)$$

Where L_S is the solar luminosity, equal to $3.85 \cdot 10^{26} \text{ W}$ [20].

Using Eq. 2.8 it is possible to calculate the energy ΔE transported across a surface of area A normal to the incident radiation in time Δt

$$\Delta E = WA\Delta t \quad (2.10)$$

The corresponding momentum transported by this energy, using Eq 2.6, is given by

$$\Delta p = \frac{\Delta E}{c} \quad (2.11)$$

It is now possible to define the pressure P exerted on the surface as the momentum transported per unit time and per unit area

$$P = \frac{1}{A} \left(\frac{\Delta p}{\Delta t} \right) \quad (2.12)$$

Therefore using Eq. 2.10 the pressure exerted on the surface due to momentum transported by photons is given by

$$P = \frac{W}{c} \quad (2.13)$$

If the sail has a perfectly reflecting surface the pressure is twice the value provided by Eq. 2.13. This is because of the momentum transferred by the incident photons and the reaction provided by reflected photons.

2.1.2 Solar sail as a perfect reflector

In this section the force on a perfectly reflecting sail is calculated. A simple case was considered to start evaluating the force, later a more realistic solar sail force model will be provided. Solar sail is considered as an oriented surface whose acceleration is a function of the sail attitude.

In Fig. 2.3 the direction of the reflected photons $\hat{\mathbf{u}}_r$ is shown. For a sail with a surface A and an unit normal vector $\hat{\mathbf{n}}$, the force due to photons incident along the $\hat{\mathbf{u}}_i$ direction is give by

$$\mathbf{f}_{i,SRP} = PA(\hat{\mathbf{u}}_i \cdot \hat{\mathbf{n}})\hat{\mathbf{u}}_i \quad (2.14)$$

Where the subscript i stands for incident, $A(\hat{\mathbf{u}}_i \cdot \hat{\mathbf{n}})$ is the projected area in the $\hat{\mathbf{u}}_i$ direction. The reflected photons will exert a force in the specular direction $-\hat{\mathbf{u}}_r$ but with the same magnitude

$$\mathbf{f}_{r,SRP} = -PA(\hat{\mathbf{u}}_i \cdot \hat{\mathbf{n}})\hat{\mathbf{u}}_r \quad (2.15)$$

Using the vector identity $\hat{\mathbf{u}}_i - \hat{\mathbf{u}}_r = 2(\hat{\mathbf{u}}_i \cdot \hat{\mathbf{n}})\hat{\mathbf{n}}$, the total force \mathbf{f}_{SRP} exerted on the solar sail is given by

$$\mathbf{f}_{SRP} = 2PA(\hat{\mathbf{u}}_i \cdot \hat{\mathbf{n}})^2\hat{\mathbf{n}} \quad (2.16)$$

This equation can be written in a different way, remembering that $P = \frac{W}{c}$, where c is the light velocity and W is the energy flux at a distant r_S from the Sun:

$$W = W_P \left(\frac{R_{S-P}}{r} \right)^2 \quad (2.17)$$

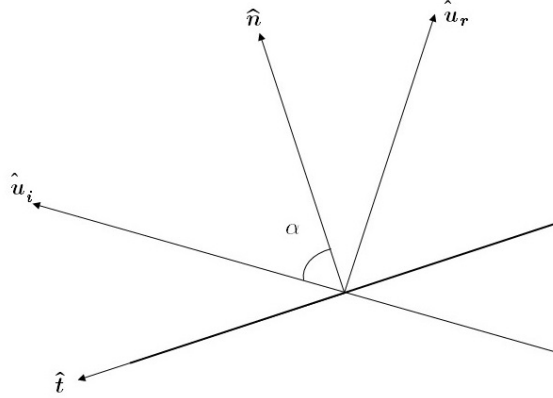


Figure 2.3: Incident photons direction and reflected photons direction.

W_P is the energy flux measured at the planet's distance from the Sun and it can be written in terms of the solar luminosity (L_S):

$$W_P = \frac{L_S}{4\pi R_P^2} \quad (2.18)$$

It is now possible to express the total force as

$$\mathbf{f}_{SRP} = 2 \frac{AW_E}{c} \left(\frac{R_{S-E}}{r} \right)^2 (\hat{\mathbf{u}}_i \cdot \hat{\mathbf{n}})^2 \hat{\mathbf{n}} \quad (2.19)$$

The solar sail acceleration due to the solar radiation pressure may now be written as

$$\mathbf{a}_{SRP} = 2 \frac{AW_E}{cm} (\cos^2 \alpha)^2 \hat{\mathbf{n}} \quad (2.20)$$

2.1.3 Optical force model

So far the sail has been considered as a perfect reflector, this means that all the photons striking the sail were reflected along $\hat{\mathbf{u}}_r$. However if a more accurate model of the acceleration due to the solar radiation pressure is required, the assumption of perfect reflectivity must be relaxed. Considering the reflectance, absorption and emissivity of the sail film, the total force exerted on the sail may be written as the sum of these three contributions

$$\mathbf{f}_{SRP} = \mathbf{f}_a + \mathbf{f}_r + \mathbf{f}_e \quad (2.21)$$

where \mathbf{f}_r is the force due to reflection, \mathbf{f}_a is the force due to absorption and \mathbf{f}_e is the force due to emission by re-radiation. The main optical properties of the sail

can be defined using the reflection coefficient \tilde{r} , absorption coefficient \tilde{a} and the transmission coefficient τ and they are related through

$$\tilde{a} + \tilde{r} + \tau = 1 \quad (2.22)$$

In this work emission by re-radiation is not considered since it is assumed that incident photons are re-emitted by reflection only [1]. This leads to $\tau = 0$ and the constraint may be written as

$$\tilde{a} = 1 - \tilde{r} \quad (2.23)$$

Considering the definition of $\hat{\mathbf{n}}$ and $\hat{\mathbf{t}}$ given in Eqs. 2.1 and 2.2, it is possible to express $\hat{\mathbf{u}}_i$ as

$$\hat{\mathbf{u}}_i = \cos \alpha \hat{\mathbf{n}} + \sin \alpha \hat{\mathbf{t}} \quad (2.24)$$

The absorption coefficient \tilde{a} takes into account the fact that a portion of the photons impacting the sail film is absorbed and the remaining part is reflected. The force exerted on the sail due to absorption can be found taking into account Eq. 2.14, considering that α is the angle between the incoming radiation and the normal vector

$$\mathbf{f}_{a,SRP} = \tilde{a}PA \cos \alpha \hat{\mathbf{u}}_i \quad (2.25)$$

where $A \cos \alpha$ is the projected sail area in direction $\hat{\mathbf{u}}_i$. Resolving this force in normal and transverse components, using Eq. 2.24

$$\mathbf{f}_{a,SRP} = \tilde{a}PA (\cos^2 \alpha \hat{\mathbf{n}} + \cos \alpha \sin \alpha \hat{\mathbf{t}}) \quad (2.26)$$

As regards the reflected photons, they generate a force equal to

$$\mathbf{f}_{r,SRP} = 2\tilde{r}PA \cos^2 \alpha \hat{\mathbf{n}} \quad (2.27)$$

Hence the acceleration due to the solar radiation pressure, on a sail with optical characteristics can be written as the sum of the acceleration along $\hat{\mathbf{n}}$ due to the absorbed and reflected photons and the acceleration along $\hat{\mathbf{t}}$ generated by the absorbed photons.

$$\mathbf{a}_{SRP} = (a_{a,SRP} + a_{r,SRP}) \hat{\mathbf{n}} + a_{a,SRP} \hat{\mathbf{t}} \quad (2.28)$$

2.2 Planetary radiation pressure

When a sail orbiting around a planet is considered, radiations coming from the planet itself, that are exerted on the sail, should be considered. For this reason in section 2.2, the model used to described the PRP force is shown and the description of the two different radiations will follow.

In the case of SRP, the source was considered as a point far away from the sail, emitting radiation. However, the sail is now close to the planet, hence the celestial body is modelled as a disc with uniform brightness. This means that it will appear equally bright when viewed from any aspect angle. Hence the variation of the direction of incidence radiation from different part of the planet will be included.

To better explain the effect of radiation pressure on a solar sail, the use of radiative transfer methods is required. The derivation by McInnes [1] will be adopted to find the expression for a PRP force with the planet modelled as a disc.

Considering an arbitrary radiation field, the properties of this field can be described as a function of both position and time. Moreover the properties can have a different distribution in direction and frequency, depending on the position within the radiation field. To describe these properties it is possible to use the specific intensity of the field. The specific intensity $I_\nu(\mathbf{r}, \mathbf{u}; t)$ of radiation at position \mathbf{r} and time t propagating in direction \mathbf{u} with frequency ν is defined to be the energy dE transported across a directed surface element $d\mathbf{A}$ in time dt into a solid angle $d\Omega$ about direction \mathbf{u} in the frequency range $(\nu + d\nu)$

$$dE = I_\nu(\mathbf{r}, \mathbf{u}; t) (\mathbf{u} \cdot d\mathbf{A}) d\Omega dt d\nu \quad (2.29)$$

As can be seen in Fig. 2.4, $\mathbf{u} \cdot d\mathbf{A}$ is the projected area normal to the direction of propagation \mathbf{u} . The radiation field is composed of individual photons. The number of photons per unit volume at position \mathbf{r} at time t and in a frequency range $(\nu + d\nu)$ propagating with speed c in a solid angle $d\Omega$ about direction \mathbf{u} can be expressed defining the photon number density function $\psi_\nu(\mathbf{r}, \mathbf{u}; t)$. Therefore

$$dN = \psi_\nu(\mathbf{r}, \mathbf{u}; t) (\mathbf{u} \cdot d\mathbf{A}) (c \cdot dt) d\Omega d\nu \quad (2.30)$$

Each photon has an energy equal to $\bar{h}\nu$, hence the energy transported is also given by

$$dE = \bar{c}\bar{h}\nu\psi_\nu(\mathbf{r}, \mathbf{u}; t) (\mathbf{u} \cdot d\mathbf{A}) d\Omega dt d\nu \quad (2.31)$$

When comparing Eqs. 2.29 and 2.31, the relation between specific intensity and photon number density function is evident

$$I_\nu(\mathbf{r}, \mathbf{u}; t) = \bar{c}\bar{h}\nu\psi_\nu(\mathbf{r}, \mathbf{u}; t) \quad (2.32)$$

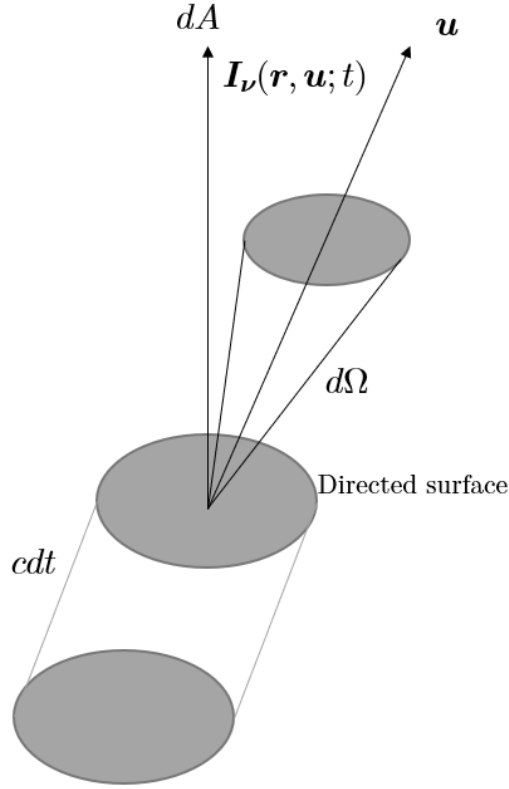


Figure 2.4: Radiation specific intensity.

Once the expression for the specific intensity is known, the SRP exerted on a radially oriented, perfectly reflecting sail at a distance r from the planet may be written as

$$P(r) = \frac{2}{c} \int_0^\infty \int_0^{2\pi} \int_0^{\theta_0} I_\nu \cos^2 \theta d\Omega d\nu, \quad d\Omega = \sin\theta d\theta d\phi \quad (2.33)$$

Where the angular radius of the disc θ_0 is given by $\sin^{-1}(R_P/r)$, as can be seen in Fig. 2.5.

Since the geometry has an azimuthal symmetry and the specific intensity is independent of r , the Eq. 2.33 then reduces to the integral

$$P(r) = \frac{4\pi}{c} I_0 \int_{\xi_0}^1 \xi^2 d\xi, \quad \xi = \cos \theta, \quad \xi_0 = \cos \theta_0 \quad (2.34)$$

where I_0 is the frequency integrated specific intensity. Performing the integration and substituting for ξ_0 it is found that

$$P(r) = \frac{4\pi}{3c} I_0 \left\{ 1 - \left[1 - \left(\frac{R_P}{r} \right)^2 \right]^{3/2} \right\} \quad (2.35)$$

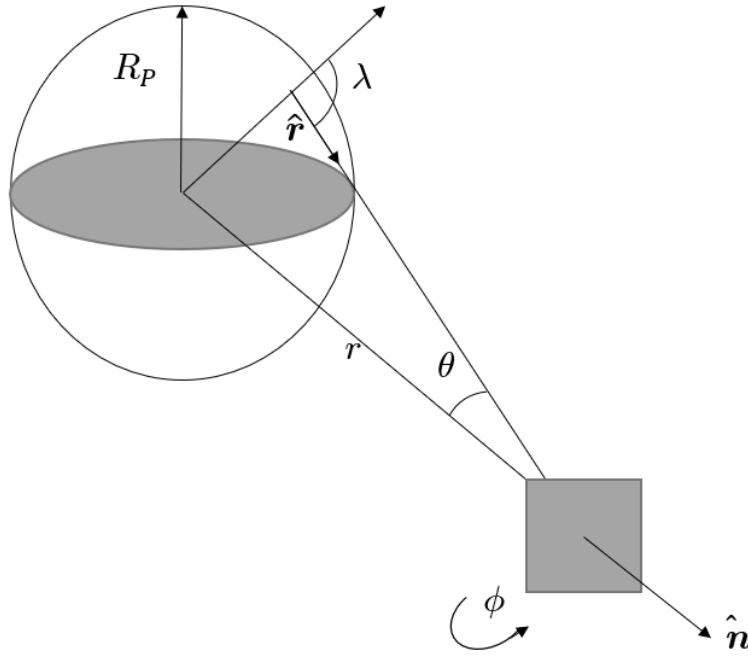


Figure 2.5: Planetary radiation pressure with a finite angular sized disc.

Now to simplify this equation, $(R_P/r)^2$ is expanded in power series and the assumption that $r \gg R_P$ is made. This is not always completely true throughout the work because the sail could be also placed at $2R_P$ of distance from the planet, but it is still useful for the simplification of the equation.

$$P(r) = \frac{2\pi}{c} I_0 \left(\frac{R_P}{r} \right)^2 + \mathcal{O} \left(\frac{R_P}{r} \right)^4 \quad (2.36)$$

However, at large values of r this expansion must match asymptotically with the expression for the radiation pressure from a distant point source

$$P(r)^* = \frac{2}{c} \left(\frac{L_P}{4\pi R_P^2} \right) \left(\frac{R_P}{r} \right)^2 \quad (2.37)$$

Hence, it is possible to define the frequency integrated specific intensity by equating Eqs. 2.36 and 2.37

$$I_0 = \frac{L_P}{4\pi^2 R_P^2} \quad (2.38)$$

When the expression for I_0 is substituted in Eq. 2.35, the planetary radiation pressure on a radially oriented solar sail from a uniformly bright, finite angular size

disc can be written as

$$P(r) = \frac{L_P}{3\pi c R_P^2} \left\{ 1 - \left[1 - \left(\frac{R_P}{r} \right)^2 \right]^{3/2} \right\} \quad (2.39)$$

Relaxing the assumption of a perfect reflector sail, the force can be modelled as a optical force, with an absorption coefficient \tilde{a} and a reflection coefficient \tilde{r} . Hence it can be resolved in normal and transverse component

$$\mathbf{f}_{a,PRP} = \tilde{a} \frac{L_P A}{3\pi c R_P^2} \left\{ 1 - \left[1 - \left(\frac{R_P}{r} \right)^2 \right]^{3/2} \right\} (\cos^2 \delta \mathbf{n} + \cos \delta \sin \delta \mathbf{t}) \quad (2.40)$$

$$\mathbf{f}_{r,PRP} = \tilde{r} \frac{L_P A}{3\pi c R_P^2} \left\{ 1 - \left[1 - \left(\frac{R_P}{r} \right)^2 \right]^{3/2} \right\} (\cos^2 \delta \mathbf{n}) \quad (2.41)$$

Where the angle δ is defined as the angle between the direction of the planetary radiation pressure ($\hat{\mathbf{r}}$) and the solar sail normal unit vector ($\hat{\mathbf{n}}$). Knowing these forces is possible to find the correspondent accelerations.

As mentioned, the radiation from the planet that we consider are of two types: the first one is the black-body radiation and the second one is the albedo. In the following sections the origin and the model used to describe these phenomena will be discussed.

2.2.1 Black body radiation pressure

In this study, the planet is considered as a black body in equilibrium with its environment, emitting the so called black body radiation. This means that the planet is an ideal and diffuse emitter. The energy is radiated isotropically and most of it will be in the infra red range [21]. Moreover the specific spectrum and intensity depend only on the body's temperature. Therefore the planet will emit according to the Stefan-Boltzmann Law [22]

$$L_P = 4\pi R_P^2 \sigma T_P^4 \quad (2.42)$$

where R_P is the radius of the planet, T_P is its mean temperature and $\sigma = 5.670370 \cdot 10^{-8} \text{ W}/(\text{m}^2 \text{ K}^4)$ is the Stefan-Boltzmann constant. Substituting this luminosity in Eqs. 2.40 and 2.41 we have the expression for the force due to the BBRP (\mathbf{f}_{BBRP}).

2.2.2 Albedo

The Sun emits its radiation equally in all directions and a part of it strikes the planet. Of all this amount, the planet reflects a fraction of this energy and this reflected radiation is know as Albedo. It varies with both geological and environmental features.

The calculation of the power generated due to albedo is based on the use of some factors [23]. First of all the fraction of the total radiant energy leaving the planet that arrives at the surface of the solar sail is considered by the view factor F . The sail can be oriented such that either one side is heated or both sides are heated. In the case of one side heated: $\Lambda + \phi_m \leq \pi/2$ and the view factor is expressed as

$$F = \frac{\cos \Lambda}{H^2} \quad (2.43)$$

Where $H = r/R$ and the angle $\phi_m = \sin^{-1} \frac{R}{r}$ as can be seen in the Fig. 2.6. When both sides are heated: $\frac{\pi}{2} - \phi_m < \Lambda < \frac{\pi}{2} + \phi_m$, and a view factor must be calculated for each side. The total view factor for the surface is then the sum of the two. The view factors for each side are given by

$$F = \frac{2}{\pi} \left[\frac{\pi}{4} - \frac{\sin^{-1} \left[\frac{(H^2 - 1)^{1/2}}{H \sin \Lambda} \right]}{2} + \frac{1}{2H^2} \left\{ \cos \Lambda \cos^{-1} \left[- (H^2 - 1)^{1/2} \cot \Lambda \right] - (H^2 - 1)^{1/2} [1 - H^2 \cos^2 \Lambda]^{1/2} \right\} \right] \quad (2.44)$$

Moreover ζ is defined as the fraction of solar radiation striking the Earth that is reflected into space. It varies both geographically and seasonally, however using $\zeta = 0.36$ gives good approximation. Moreover albedo occurs over only the daylight side of the planet, and it varies as the cosine of the reflection angle ϑ shown in the Fig. 2.7. It is now possible to calculate the albedo heating as

$$q_a = W_P \zeta F \cos \vartheta \quad (2.45)$$

Where W_P is the solar flux at planet orbit. This heat is in $[\text{W}/\text{m}^2]$, but in the equation of the force (Eqs. 2.40 and 2.41) a power is considered, hence this flux should be multiply by the disc surface, that is the area struck by the solar radiation and that reflects the radiation back into space.

It is now possible to express the luminosity due to the albedo as

$$L_P = q_a \pi R_P^2 \quad (2.46)$$

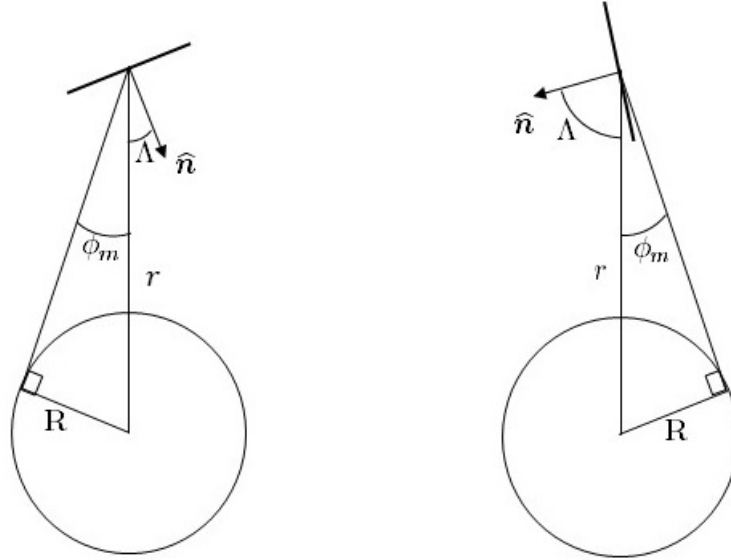


Figure 2.6: Planet heating geometry for a view factor calculation: on the left one side is heated, on the right both sides are heated.

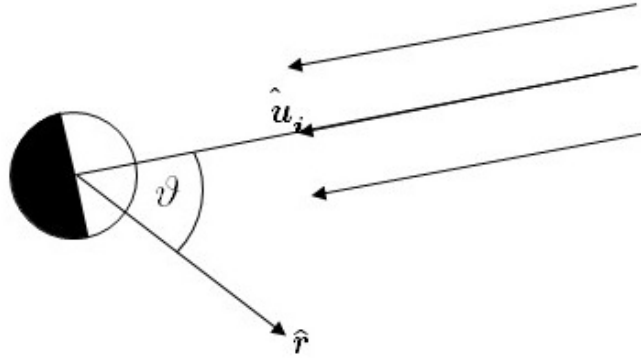


Figure 2.7: Reflection angle.

This two contributions expressed in Eqs. 2.42 and 2.46 can then be used in the equation of the forces Eqs. 2.40 and 2.41 and they will express the force due to BBRP and ARP respectively and the sum of them is the contribution due to the PRP.

The total acceleration experienced by the sail, when it is out of the eclipse region, for negative x and $y \in [-R_P, R_P]$, can be written as

$$\mathbf{a} = (a_{a,SRP} + a_{r,SRP} + a_{a,PRP} + a_{r,PRP}) \hat{\mathbf{n}} + (a_{a,SRP} + a_{a,PRP}) \hat{\mathbf{t}} \quad (2.47)$$

When the sail is in eclipse, the elements due to the SRP are equal to zero and the sail is subject to the PRP only.

Chapter 3

Methodology

In this chapter the methodology used in this work is explained. Knowing the expressions for the forces, hence the accelerations, exerted on the sail, the behaviour of a planetary sail subject to SRP and PRP can be studied. The work focuses on finding the attitude angle σ that enables the sail to have a desired acceleration along a given direction. Once this angle is known, it could be used in the dynamics of the sail to perform different trajectories. In this work it has been decided to maximise the magnitude, radial and transversal components of the acceleration, since they could be used in the dynamics of the sail.

In Section 3.1, the investigation of an analytical law which describes the attitude angle that leads to a maximum transversal acceleration is performed. Since the complexity of this law, it has been decided to proceed using a numerical approach. This numerical approach is described in Section 3.2. In this case the sail is placed in a point in the vicinity of the planet. Its attitude angle changes from 0 to 2π and for each angle the corresponding acceleration along a given direction is found. Among these values, the requested one is picked and the corresponding angle is chosen as the optimal attitude in that point.

3.1 Analytical law

The first step for this study is to find an analytical law that shows the attitude of the sail for maximising the acceleration along a given direction.

For simplicity it has been decided to use an explanatory case study in which the angle σ that maximises the transversal acceleration has to be found.

The angle σ ranges between 0 and 2π so that all the possible attitude of the sail are considered. To find the relation expressing the value of σ that maximises the transversal acceleration, all the accelerations due to SRP and PRP should be expressed as function of this angle, the derivation of the transversal acceleration will

be performed and it will be equated to zero to find the attitude corresponding to the maximum transversal acceleration. For this reason the other angles α and δ should also be expressed as functions of σ .

To simplify this problem three assumptions are used:

- Since the sail is in a planet-centred orbit, the distance from the Sun is large and the solar rays can be considered parallel to the x -axis (Fig. 3.1). Hence the pitch angle α can be written as $\alpha = \pi - \sigma$.
- In the rest of this work, the acceleration due to reflection and absorption of the photons is considered (Eq. 2.47). The latter leads to an acceleration with a component along $\hat{\mathbf{t}}$. Since this acceleration is 1 ÷ 2 orders of magnitude smaller than the acceleration along $\hat{\mathbf{n}}$, it is possible to neglect it.
- The contribution due to albedo is neglected too, since its luminosity is 2 orders of magnitude smaller than the BBR one.

Therefore the pitch angle α and the angle δ can be expressed as

$$\alpha = \pi - \sigma \tag{3.1}$$

$$\delta = \sigma - \theta \tag{3.2}$$

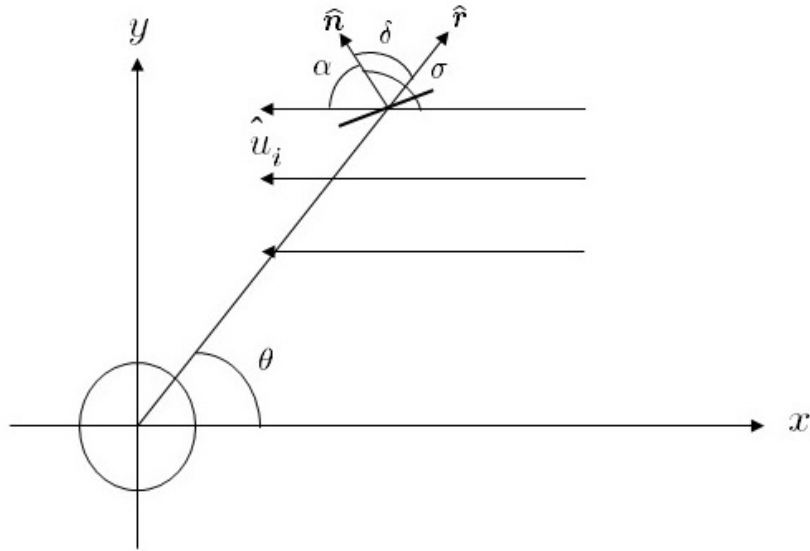


Figure 3.1: Reference frame with angles.

where θ is the angle between the radial direction and the x -axis. First the expression for the transversal acceleration is found

$$a_\theta = -a_x \sin\theta + a_y \cos\theta = -(a_{nx} + a_{tx}) \sin\theta + (a_{ny} + a_{ty}) \cos\theta \quad (3.3)$$

Where the subscript θ expresses the transversal direction, a_{nx} is the acceleration along the normal to the sail surface, projected along the x -axis, a_{tx} is the acceleration along the transversal to the sail surface, projected along the x -axis and so on. Remembering that the acceleration along $\hat{\mathbf{t}}$ is neglected, the transversal acceleration can be written as

$$a_\theta = -a_n \cos\sigma \sin\theta + a_n \sin\sigma \cos\theta \quad (3.4)$$

The components of the acceleration along the direction $\hat{\mathbf{n}}$ can be written as the sum of different contributions due to the SRP and the BBRP.

$$a_n = a_{na,SRP} + a_{nr,SRP} + a_{na,BBRP} + a_{nr,BBRP} \quad (3.5)$$

where subscript a and r refers to the contribution due to absorption and reflection, respectively. These accelerations can be expressed as

$$a_{na,SRP} = \tilde{a} W_E \frac{A}{cm} \left(\frac{R_{S-P}}{r} \right)^2 \cos^2 \alpha \quad (3.6)$$

$$a_{nr,SRP} = 2\tilde{r} W_E \frac{A}{cm} \left(\frac{R_{S-P}}{r} \right)^2 \cos^2 \alpha \quad (3.7)$$

$$a_{na,BBRP} = \tilde{a} \frac{L_E A}{3\pi cm R_P^2} \left\{ 1 - \left[1 - \left(\frac{R_T}{r} \right)^2 \right]^{3/2} \right\} \cos^2 \delta \quad (3.8)$$

$$a_{nr,BBRP} = 2\tilde{r} \frac{L_E A}{3\pi cm R_P^2} \left\{ 1 - \left[1 - \left(\frac{R_T}{r} \right)^2 \right]^{3/2} \right\} \cos^2 \delta \quad (3.9)$$

Introducing these accelerations in Eq. 3.3 and expressing all the angles as function of σ (Eqs. 3.1 and 3.2), the transversal acceleration may be written as

$$a_\theta = (2\tilde{r} + \tilde{a}) \left[\frac{L_E A}{3\pi cm R_P^2} \left\{ 1 - \left[1 - \left(\frac{R_T}{r} \right)^2 \right]^{3/2} \right\} \cos^2 (\sigma - \theta) + W_E \frac{A}{cm} \left(\frac{R_{S-P}}{r} \right)^2 \cos^2 \sigma \right] (\sin \sigma \cos \theta - \cos \sigma \sin \theta) \quad (3.10)$$

To find the expression of the attitude angle that maximises the acceleration along the transversal acceleration, this equation will be derived with respect to σ .

$$\begin{aligned} \frac{da_\theta}{d\sigma} = & \frac{1}{3cm\pi r^2 R_P^2} \left(A(2\tilde{r} + \tilde{a}) \cos(\sigma - \theta) \left(3\pi R_{S-P}^2 R_T^2 W_E \cos^2 \sigma + L_E r^2 \right. \right. \\ & \left. \left. \left(1 - \left(1 - \frac{R_P^2}{r^2} \right)^{3/2} \right) \cos^2(\sigma - \theta) \right) - 2A(2\tilde{r} + \tilde{a}) \sin(\sigma - \theta) \right. \\ & \left. \left(3\pi R_{S-P}^2 R_T^2 W_E \cos \sigma \sin \sigma + \frac{1}{2} L_E r^2 \left(1 - \left(1 - \frac{R_P^2}{r^2} \right)^{3/2} \right) \sin 2(\sigma - \theta) \right) \right) \end{aligned} \quad (3.11)$$

Clearly, even with the assumptions that were made, it is not easy to solve $\frac{da_\theta}{d\sigma} = 0$ since it is a transcendental equation. For this reason it has been decided to plot the function Eq. 3.10 for different points around the planet to analyse the behaviour of the transversal acceleration for different values of $\sigma = [0, 2\pi]$. The chosen points are $A = [-2R_P, 2R_P]$, $B = [2R_P, 2R_P]$, $C = [2R_P, -2R_P]$ and $D = [-2R_P, -2R_P]$. As can be seen in Fig. 3.2, the function has six equilibrium points with a global maximum point that changes in every point. This means that the use of a gradient-based method would not be able to reliably locate the positions of the zeros for this function. Since it is not easy to find analytically the value of σ that maximises the transversal acceleration, a numerical approach has been used throughout the study.

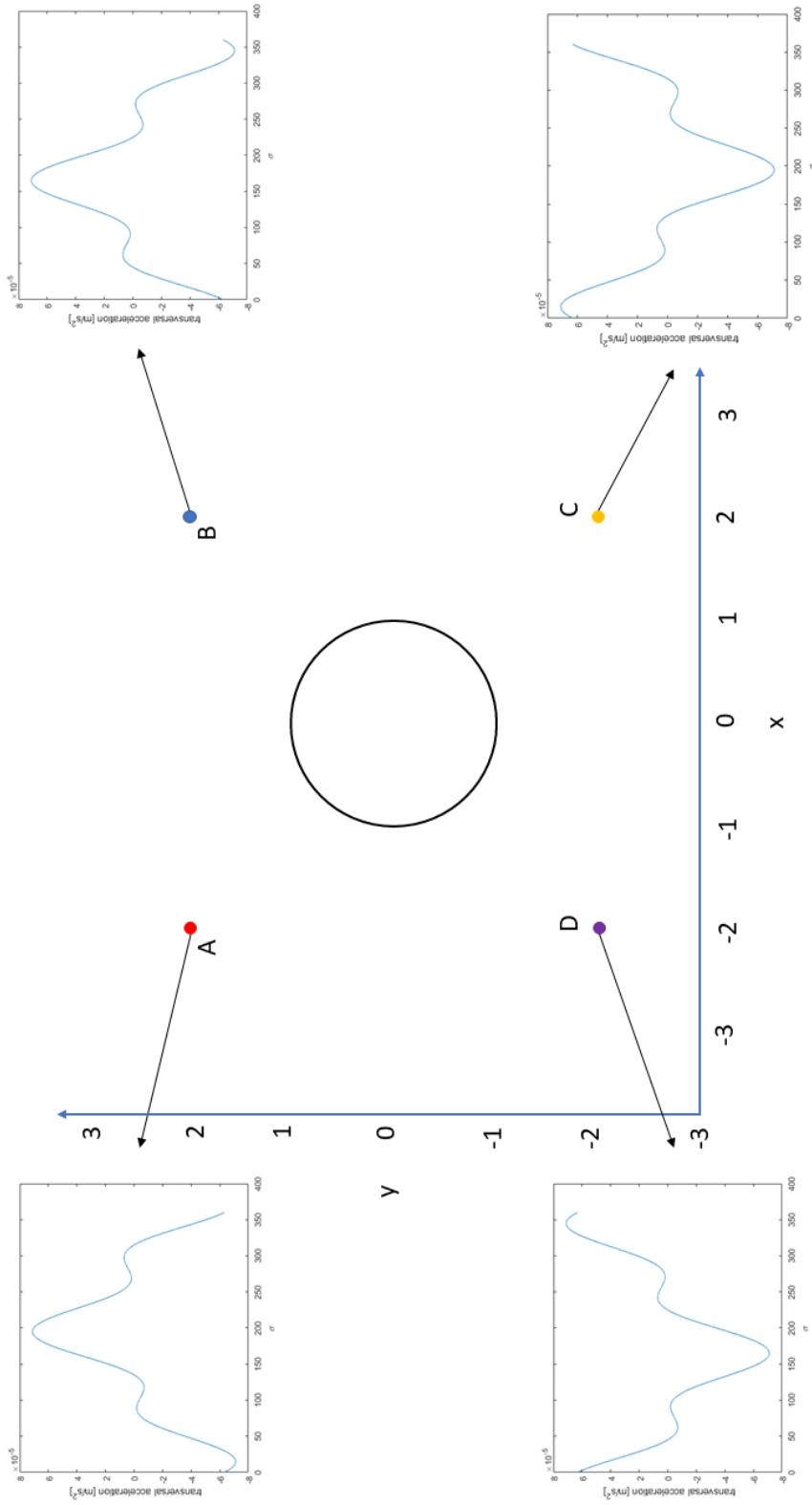


Figure 3.2: Behaviour of the transversal acceleration in different points around the planet

3.2 Numerical approach

Once all the forces have been modelled and it has been decided to proceed using a numerical approach.

The analysis started with a sail in a point with an attitude angle σ equal to zero. Subsequently 1000 values of σ from 0 to 2π are scanned and the corresponding acceleration along a given direction is calculated for each angle. Among these accelerations, the one that satisfies the requirements is picked and the corresponding angle is chosen as the optimal attitude for the sail in that point. Requirements varies according to the different study-cases, where a maximisation or minimisation of the acceleration along a given direction would be required. They will be presented in details in Chapter 4 and 5.

The approach used in a point is then applied for a grid of points (500×500) around a planet. Since the atmospheric presence is not considered, points that are at least 400 km above the planet surface are taken into account. During this work a sail with a sail loading $\sigma^* = 0.1 \text{ kg/m}^2$ is considered. The ratio of the resulting acceleration to the specific characteristic acceleration ($a_{0,s}$) of the planet is considered as the main parameter. Hence, results do not depend on the sail geometry and they are valid for every flat sail regardless of its mass or surface.

The analysis has been conducted around four planets:

- Mercury
- Venus
- Earth
- Mars

For each planet the specific characteristic acceleration is calculated using Eq. 2.3, where P_{SRP} is the solar radiation pressure at the mean distance between the Sun and the planet. Results are presented in Table 3.1.

To add the contribution of the BBRP, the luminosity should be calculated according to the Stefan-Boltzmann law (Eq. 2.42). Values of planetary radius (R_P), mean temperature of the planet ($T_{m,P}$) and the corresponding luminosity (L_{BBRP}) are shown in Table 3.1.

As for the pressure due to albedo, it is not possible to calculate a general value since it changes both with the point and the attitude angle of the sail (Eq. 2.45). However the value of the solar flux in planet orbit is reported in Table 3.1 and it is used in the calculation of the luminosity.

Planet	Mercury	Venus	Earth	Mars
P_{SRP} [N/m ²]	$3.04 \cdot 10^{-5}$	$8.72 \cdot 10^{-6}$	$4.56 \cdot 10^{-6}$	$1.96 \cdot 10^{-6}$
$a_{0,s}$ [m/s ²]	$5.78 \cdot 10^{-4}$	$1,65 \cdot 10^{-4}$	$8,66 \cdot 10^{-5}$	$3,73 \cdot 10^{-5}$
R_P [m]	$2430 \cdot 10^3$	$6070 \cdot 10^3$	$6378 \cdot 10^3$	$3390 \cdot 10^3$
$T_{m,P}$ [K]	440.15	735.15	279.00	210.37
L_{BBRP} [W]	$1.5791 \cdot 10^{17}$	$1.6679 \cdot 10^{18}$	$1.7562 \cdot 10^{17}$	$1.6038 \cdot 10^{16}$

Table 3.1: Solar radiation pressure at the mean distance between the Sun and the planet, specific characteristic acceleration, planet radius, planet mean temperature, luminosity due to the BBRP and solar flux in orbit for different planets.

Once all these parameters have been evaluated, the study is conducted for two kinds of sail with different optical properties for the front and back side of the sail film. The first is a single-side reflective coating sail in which the front side has a reflection coefficient $\tilde{r}_f = 0.9$ and the back side has $\tilde{r}_b = 0$. This means that all the photons are absorbed by the back side of the sail. The second sail instead has a double-side reflective coating, with a reflection coefficient equal to $\tilde{r} = 0.9$ for both sides. In Table 3.2 the values of the optical coefficient used throughout the work are summarised.

Kind of sail	\tilde{r}_f	\tilde{a}_f	\tilde{r}_b	\tilde{a}_b
Single-side coated	0.9	0.1	0	0.9
Double-side coated	0.9	0.1	0.9	0.1

Table 3.2: Value of the reflection and absorption coefficients for the back- and front-side of a single- and double-side reflective coating sail.

Results obtained following this methodology are presented in Chapter 4. The acceleration is maximised in magnitude, along the radial direction and along the transversal direction.

For each case-study different contributions are considered:

- SRP only;
- SRP+BBRP;
- SRP+ARP;
- SRP+PRP.

Results are shown for four planets and considering the two kinds of sail previously described.

Chapter 4

Results

In this chapter results are shown considering the maximisation of the magnitude of the acceleration in Section 4.1 and the radial and transversal acceleration in Sections 4.2 and 4.3, respectively. For each case the contribution of the SRP only, SRP+BBRP, SRP+ARP and SRP+PRP is analysed.

Results are presented using two kinds of plots: one shows the direction of the sail unit normal vector $\hat{\mathbf{n}}$ as an oriented arrow and the other shows the contour of the sail acceleration over the characteristic acceleration.

4.1 Maximum magnitude of the acceleration

Results for a maximum acceleration magnitude are presented in this section. As already mentioned the acceleration due to absorption and reflection is considered in this study. For this reason the direction of the sail acceleration is not all along the $\hat{\mathbf{n}}$ direction, since the absorbed photons generate an acceleration along $\hat{\mathbf{t}}$, too. Hence the final acceleration can be written as: $a = \sqrt{a_n^2 + a_t^2}$ and it should be maximised.

4.1.1 SRP

In this section the results obtained for a sail subject to SRP only are shown. These results are used as terms of reference throughout the work. Results obtained with the addition of a new contribution are always compared with the ones presented in this section. This helps to understand if any consistent difference arises and to evaluate any possible improvement in terms of sail performance.

Results are shown for a sail placed in a grid of points around four planet: Earth, Mercury, Mars and Venus.

Earth

Fig. 4.1 shows the results for a single-side coating planetary sail in the vicinity of the Earth. In particular Fig. 4.1a presents the direction of the sail normal when the sail is placed in a grid of 30 points included in $x \in [-2R_P, 2R_P]$ and $y \in [-2R_P, 2R_P]$. In this case the sail is oriented with an attitude angle $\sigma = 180$ deg in every point of the grid. As regards the acceleration, Fig. 4.1b shows the contour of the ratio a_{SRP}/a_0 . Since the range of the grid is in a much smaller scale with respect to the distance from the Sun, the variation of this parameter is limited. In the eclipse region instead the sail is subject to no force and it is meaningless to find an attitude to maximise the absolute acceleration.

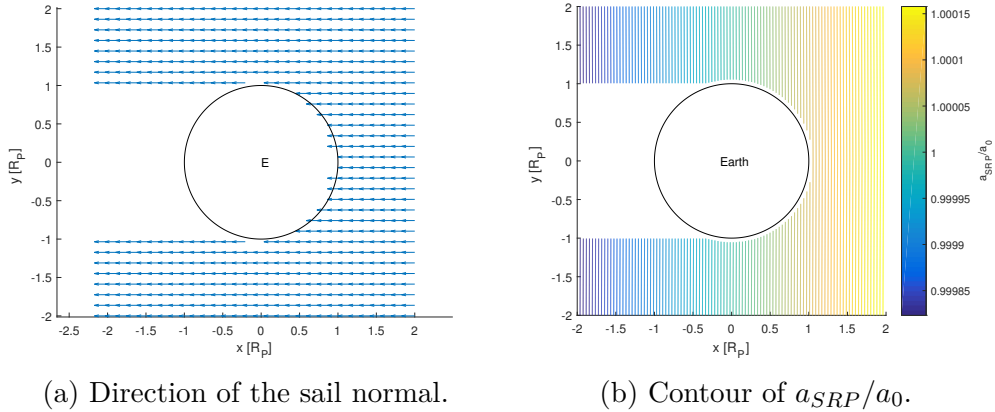


Figure 4.1: Maximisation of the magnitude of the acceleration, for a single-side coating sail around the Earth subject to SRP.

Mercury

In the case of a sail in the vicinity of Mercury, results are shown in Figs. 4.2a and 4.2b. The behaviour of the sail is similar to one around the Earth (Fig. 4.5), with an attitude angle σ always equal to 180 deg and with no large variation of the parameter a_{SRP}/a_0 .

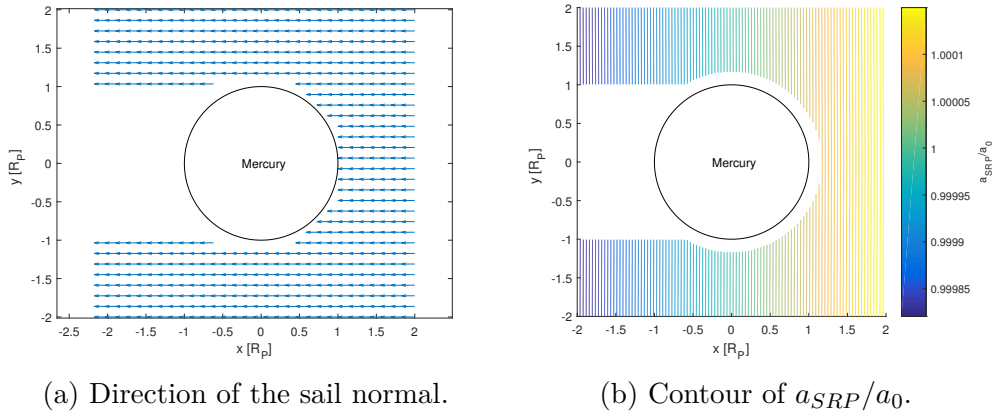


Figure 4.2: Maximisation of the magnitude of the acceleration, for a single-side coating sail around Mercury subject to SRP.

Mars

When the sail is around Mars, it experiences a lower SRP due to the greater distance from the Sun. Nevertheless, results are similar to the two previous cases. Fig. 4.3a shows a sail facing the Sun in every point of the grid and Fig. 4.3b presents a very little variation of the ratio a_{SRP}/a_0 , due to the greater distance from the Sun.

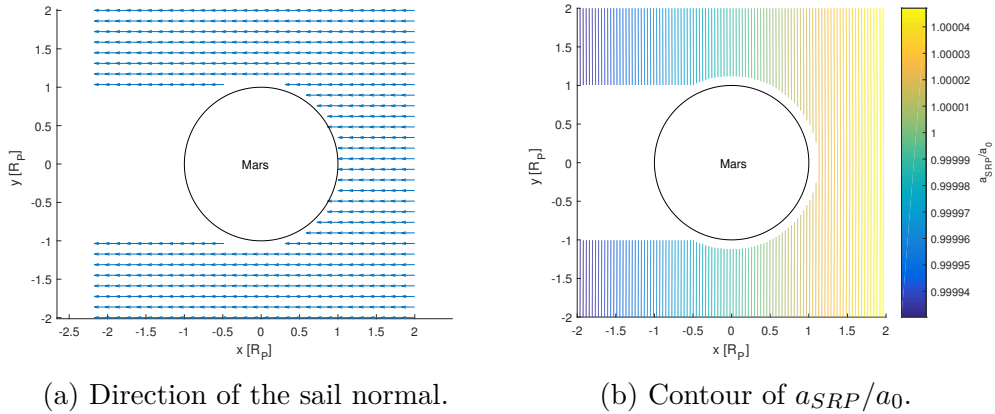


Figure 4.3: Maximisation of the magnitude of the acceleration, for a single-side coating sail around Mars subject to SRP.

Venus

The results for a sail in the vicinity of Venus considering the presence of SRP only, are shown in this section. The comparison between these results and the ones

considering the contribution of the planet are used to quantify the effect of the PRP. The case of a maximum magnitude acceleration is presented in Fig. 4.4. In this case the sail is always oriented with an angle $\sigma = 180$ deg, facing the Sun. As in the case around the Earth, the ratio a_{SRP}/a_0 has an almost constant trend.

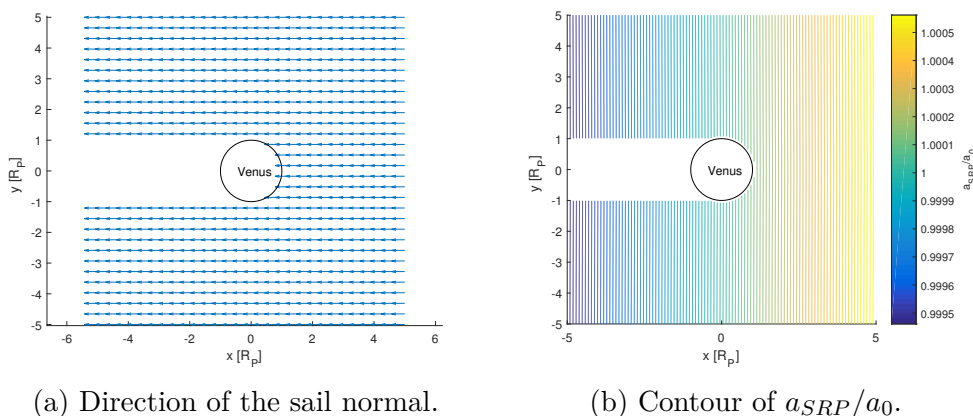


Figure 4.4: Maximisation of the magnitude of the acceleration, for a single-side coating sail around Venus subject to SRP.

4.1.2 SRP+BBRP

In this section the contribution due to the BBRP is added, using the parameters shown in Table 3.1. It has been decided that in the case of a maximum magnitude of the acceleration this is the only additional contribution considered, since it has the greatest luminosity.

Earth

In Fig. 4.5a the direction of the unit normal vector $\hat{\mathbf{n}}$ is presented. The sail is facing the Sun with an attitude angle of ~ 180 deg, similarly to the case SRP only showed in Fig. 4.1a. However, when the sail is in the eclipse region, it is oriented radially, where the acceleration is provided just by the PRP. Fig. 4.5b shows the contour of the ratio $a_{SRP+BBRP}/a_0$, here the increment respect to the characteristic acceleration is experienced everywhere. When the sail is in eclipse even if the acceleration is decreased, there is still the contribution given by the planet that is not considered in the case SRP only. Comparing Figs. 4.5b and 4.1b, the maximum contribution of the BBRP can be calculated, knowing that the highest value of the ratio is 1.1185 in case SRP+BBRP and 1.0002 for the case SRP only. This leads to a percentage increment of 11.82%.

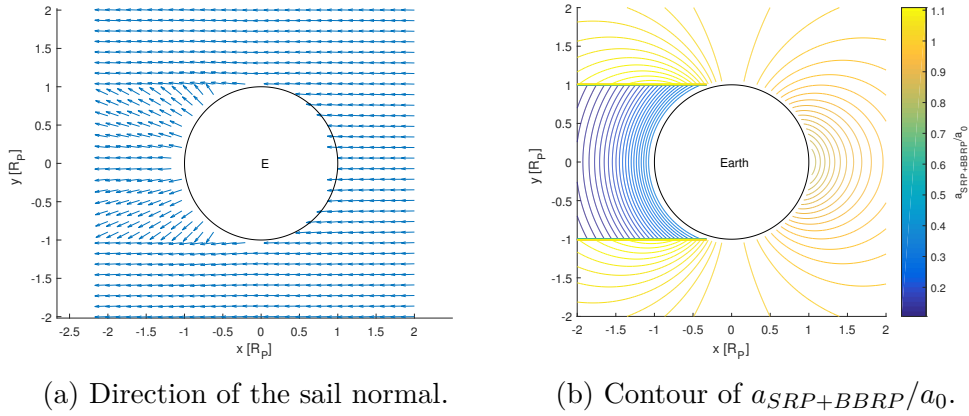


Figure 4.5: Maximisation of the magnitude of the acceleration, for a single-side coating sail around the Earth subject to SRP and BBRP.

The case of a double-side reflective coating sail is briefly presented in Fig. 4.6. In this case the unit normal vector (Fig. 4.6a) is specular with respect to the single-side reflective coating case, with no consistent differences. In Fig. 4.6b there is a slightly difference when compared to Fig. 4.5b just in the region out of the umbra, near the planet, where the BBRP causes a decrease of the acceleration experienced by the sail.

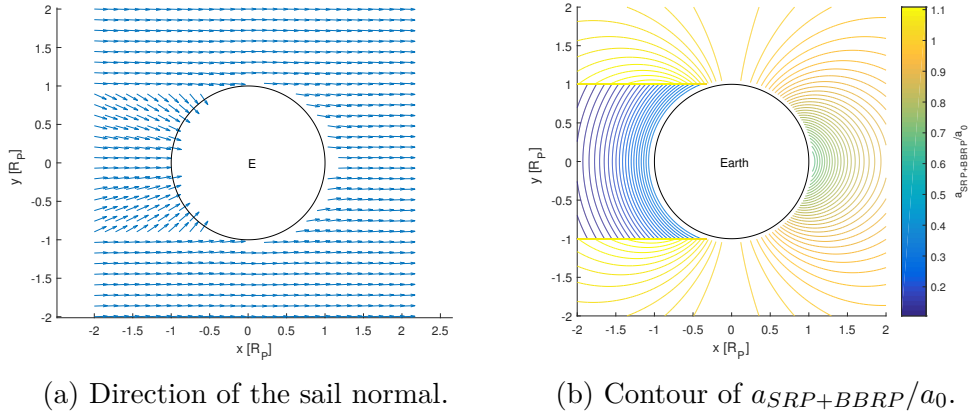


Figure 4.6: Maximisation of the magnitude of the acceleration, for a double-side coating sail around the Earth subject to SRP and BBRP.

Mercury

In the case of a sail in the vicinity of Mercury, it is possible to calculate the contribution of the BBRP. The luminosity of this planet is smaller than the Earth’s one, as can be seen in Table 3.1, so the results are just shown in the case of a maximum absolute acceleration with a single-side reflective coating sail. Figs. 4.7 shows the results in the case SRP+BBRP. The behaviour of the sail around Mercury is really similar to one around the Earth (Fig. 4.5). What changes is that in this case the increase considering the BBRP is decreased at 10.89%. Since the planet is closer to the Sun, the contribution given by the SRP is greater and the sail experienced the effect of the BBRP less than in a Earth-centred orbit.

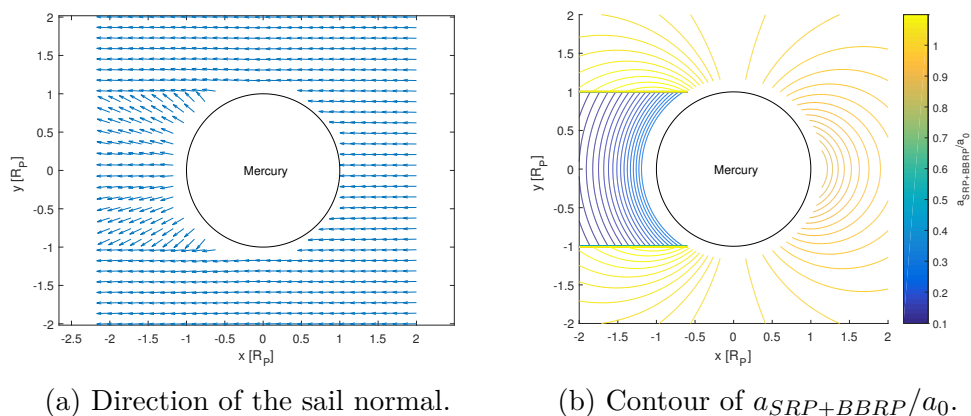


Figure 4.7: Maximisation of the magnitude of the acceleration, for a single-side coating sail around Mercury subject to SRP and BBRP.

Mars

Since the contribution of the SRP is smaller with respect to the previous cases, one could expect that the relative effect of BBRP would be greater. However it has been found that this does not occurs, since the planet presents the lowest BBRP luminosity (Table 3.1). The comparison between the cases SRP only and SRP+BBRP shows that the acceleration increases of 8.67% in the latter case. Further studies of this case are not relevant since the similarity with the results obtained for the Earth and the smaller effects of the planetary pressure .

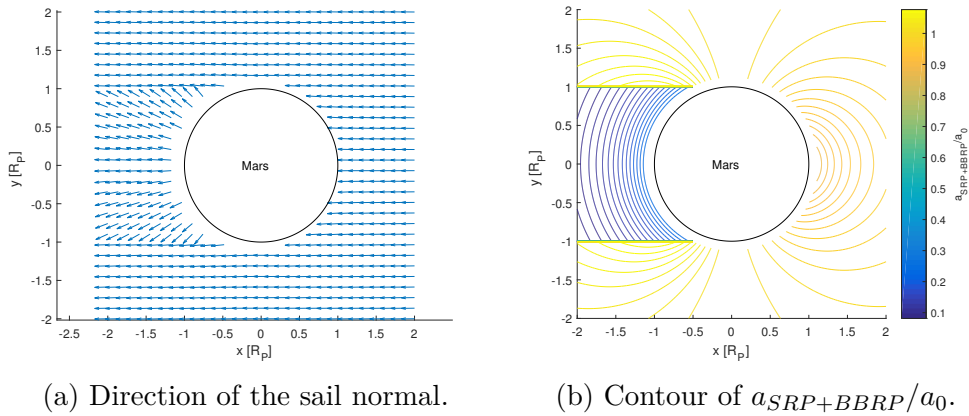


Figure 4.8: Maximisation of the magnitude of the acceleration, for a single-side coating sail around Mars subject to SRP and BBRP.

Venus

Venus has a great luminosity due to its high mean temperature (Table 3.1). As a consequence the BBRP, and the PRP in general, can give an important contribution to the acceleration of the sail. In this case, as already done for the Earth, the results will be shown for a wider grid of points with $x \in [-5R_P, 5R_P]$ and $y \in [-5R_P, 5R_P]$ and the accelerations will be shown in ratio with the specific characteristic acceleration a_0 , shown in Table 3.1.

Figs 4.9 and 4.10 show the results for a sail in the vicinity of Venus in the case considering SRP+BBRP with a maximum magnitude of the acceleration. Results are showing that BBRP is the dominating contribution to the thrust of the sail up to four times the radius of the planet (Fig. 4.9a). If the SRP is considered as the only contribution (Fig. 4.4a) the sail has a completely different orientation, always facing the Sun with an attitude angle equal to 180 deg. The addition of the BBRP leads to a radial orientation of the sail and to an increase of the acceleration around of 700% for the points closer to the planet. Moreover Fig. 4.9b shows that there is almost no variation from the light to the umbra region, with a gap that gets smaller when the sail is close to the planet. This means that the sail does not experience a sudden change when placed in the eclipse region.

When a double-side reflective coating sail is considered, the results are similar to the previous case, with the orientation of the sail rotates of 180 deg (Fig. 4.10a). As regards the absolute acceleration, the sail experiences greater acceleration when placed in the points at about 5 planet radii along the x -axis, since in this case the negative contribution given by the Sun is contrasted by the PRP (Fig. 4.10b).

Table 4.1 presents the percentage increment obtained adding the contribution of the BBRP to the maximisation of the acceleration magnitude.

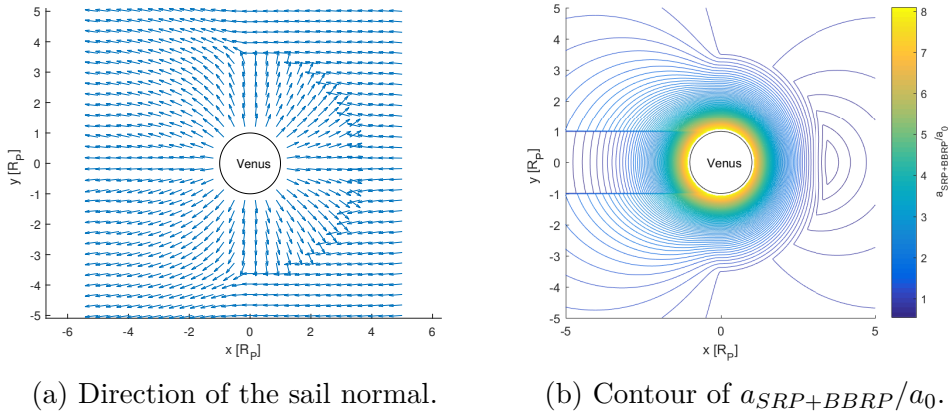


Figure 4.9: Maximisation of the magnitude of the acceleration, for a single-side coating sail around Venus subject to SRP and BBRP.

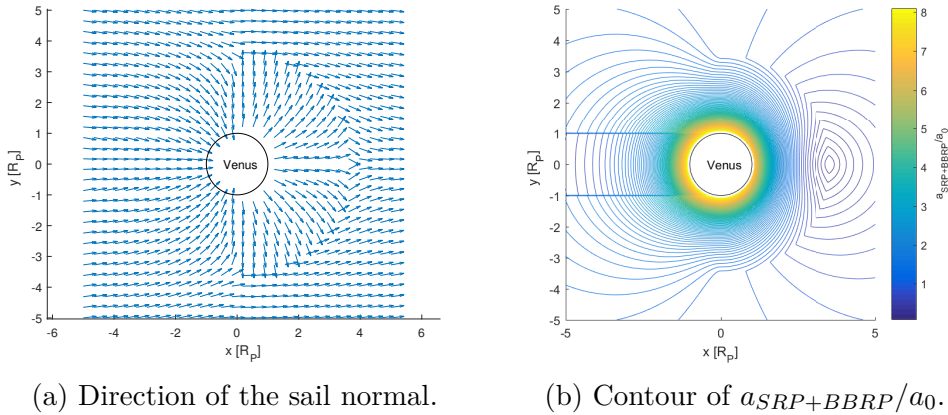


Figure 4.10: Maximisation of the magnitude of the acceleration, for a double-side coating sail around Venus subject to SRP and BBRP.

Planet	$a_{SRP}/a_{0,s}$	$a_{SRP+BBRP}/a_{0,s}$	Percentage increase
Earth	1.0002	1.1185	11.8%
Mercury	1.0002	1.1091	10.89%
Mars	1.00004	1.0868	8.67%
Venus	1.0001	8.1704	712%

Table 4.1: Value of the ratio $a_{SRP}/a_{0,s}$, $a_{SRP+BBRP}/a_{0,s}$ and corresponding percentage increase.

4.2 Maximum radial acceleration

In this section the maximisation of the acceleration along the radial direction is performed. As already done before, results are shown considering different contributions and different planets. However, since the similar results obtained for Earth,

Mercury and Mars, it has been decided to proceed the study considering just a sail in the vicinity of the Earth and Venus.

4.2.1 SRP

The contribution given by the SRP is presented in the following sections.

Earth

The results in the case of a maximum radial acceleration is presented in Fig. 4.11. Fig. 4.11a shows the direction of the sail normal. It presents a region of null acceleration for the points in the range $x \in [1R_P, 2R_P]$ and $y \in [-1R_P, 1R_P]$ where the attitude angle σ is equal to 90 or 270 deg. In this area the Sun gives a negative contribution along the radial direction, for this reason it is preferred to have a null acceleration than a negative one. Moreover Fig. 4.11b shows that the greatest radial acceleration can be found for points with $x \in [-2R_P, -1R_P]$, where the Sun gives a positive contribution along the radial direction.

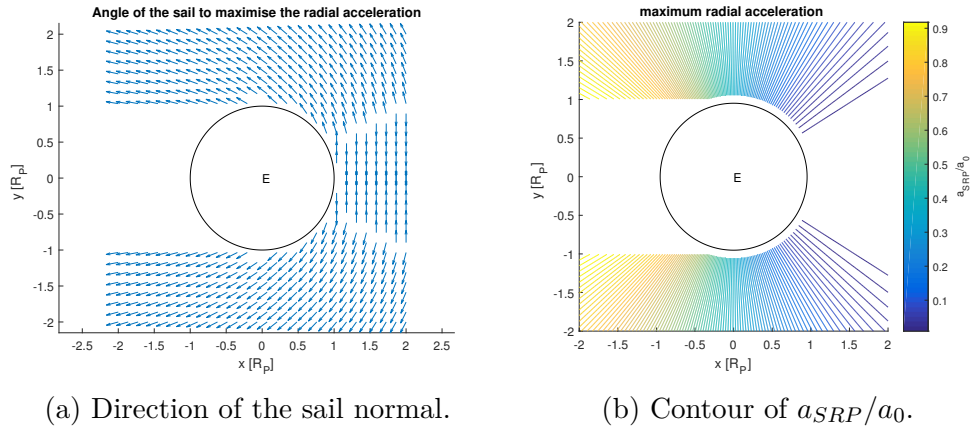


Figure 4.11: Maximisation of radial acceleration, for a single-side coating sail around Earth subject to SRP.

Venus

Fig. 4.12 shows the results for the maximum radial acceleration. As already stated for the Earth, maximum radial acceleration can be found in the left part of the grid (Fig. 4.12b) while a null acceleration is experienced, to avoid a negative one, when the sail is placed in points with $x \in [1R_P, 5R_P]$ and $y \in [-2R_P, 2R_P]$.

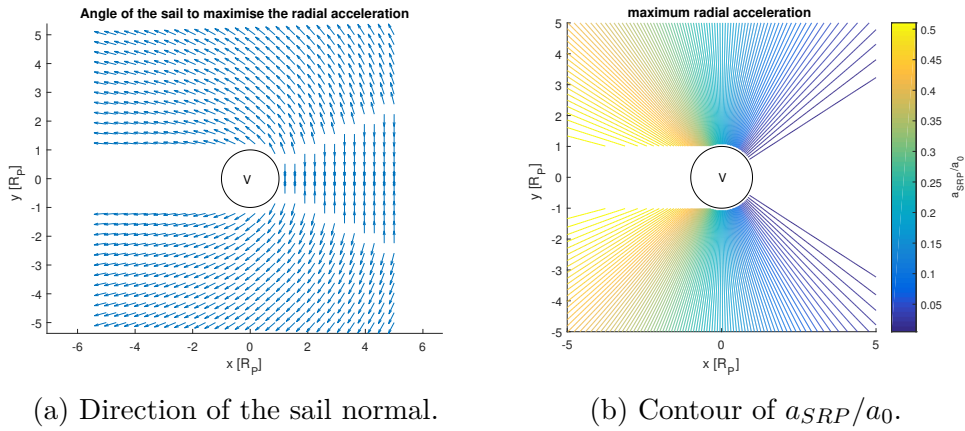


Figure 4.12: Maximisation of radial acceleration, for a single-side coating sail around Venus subject to SRP.

4.2.2 SRP+BBRP

Adding the contribution of the BBRP, it is possible to obtain the results presented later. Moreover for this case two kinds of sail are considered: single-side reflective coating sail and double-side reflective coating sail.

Earth

Results presented in this section consider a sail orbiting around the Earth subjected to SRP and BBRP. The value of the Earth luminosity can be found in Table 3.1. Fig. 4.13 shows the results for a maximum radial acceleration. When comparing them with Fig. 4.11, some differences can be found:

- the sail is oriented radially in the umbra region due to the contribution of the BBRP
- the sail has an attitude angle that is no more precisely 90 or 270 deg in the points with positive x and $y \in [-1R_P, 1R_P]$. This leads to an acceleration greater than zero when the BBRP is added.
- the sail, placed at 400 km from the planet surface, is oriented with a different attitude and with a greater acceleration up to one order of magnitude in the case of SRP+BBRP.

From the comparison between the two cases, an increase of 9% occurs in the region with negative x and out of the shadow.

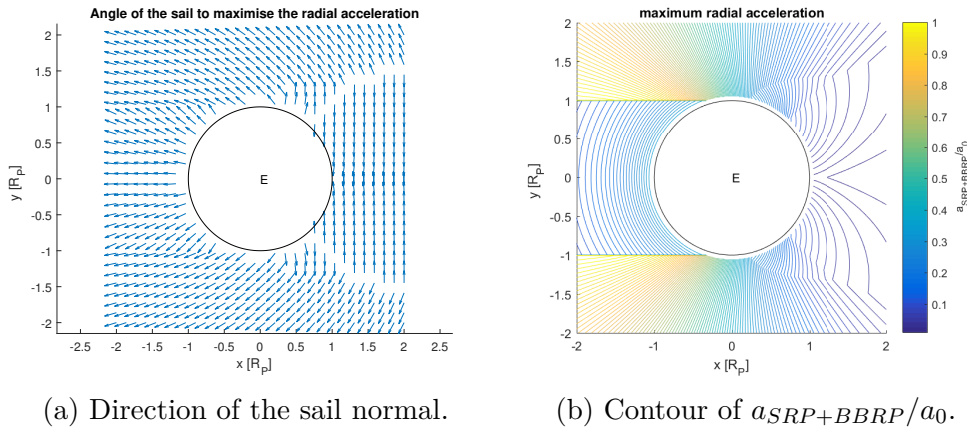


Figure 4.13: Maximisation of radial acceleration, for a single-side coating sail around Earth subject to SRP and BBRP.

When a double-side reflective coating sail is considered, the obtained results are shown in Fig. 4.14. In this case, as regards the maximisation of the radial acceleration, it is possible to notice a different behaviour with a sail with a single-side reflective coating (Fig. 4.13):

- the sail orientation is specular in the shadow region, since there is no difference between the front and back side of the sail.
- the sail has an attitude angle equal to 90 or 270 deg, with a null acceleration in the point with a positive x and y in the range $[-1R_P, 1R_P]$, in this case the acceleration is null to avoid a negative one.

Also in this case the increment of the acceleration due to the BBRP is equal to 9%, this means that the consideration of a double-side reflective coating does not change significantly the results.

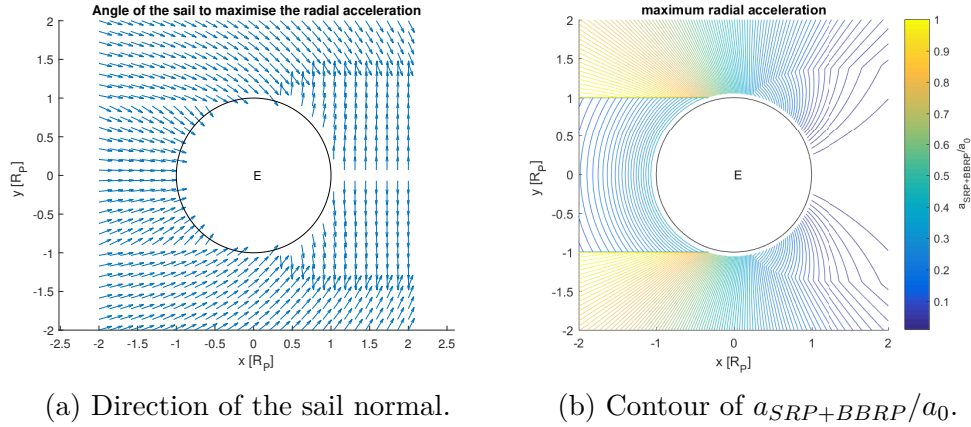


Figure 4.14: Maximisation of radial acceleration, for a double-side coating sail around Earth subject to SRP and BBRP.

Venus

Considering a single-side reflective coating sail, results for a maximum radial acceleration can be found in Fig. 4.15. The dominating contribution is the BBRP, in fact comparing the Figs. 4.15 and 4.12 many differences can be found:

- For most of the grid the sail is oriented radially. This means that the BBRP is by far the main contribution, not only in the eclipse region.
- The greatest acceleration is experienced when the sail is placed close to the planet and not in the right part of the grid as in the case with SRP only.
- The ratio $a_{SRP+BBRP}/a_0$ is eight times greater than the one obtained when the only SRP is considered.
- There is no clear difference when the sail is placed in the eclipse region since the contribution given by the Sun is minor than the BBRP one.

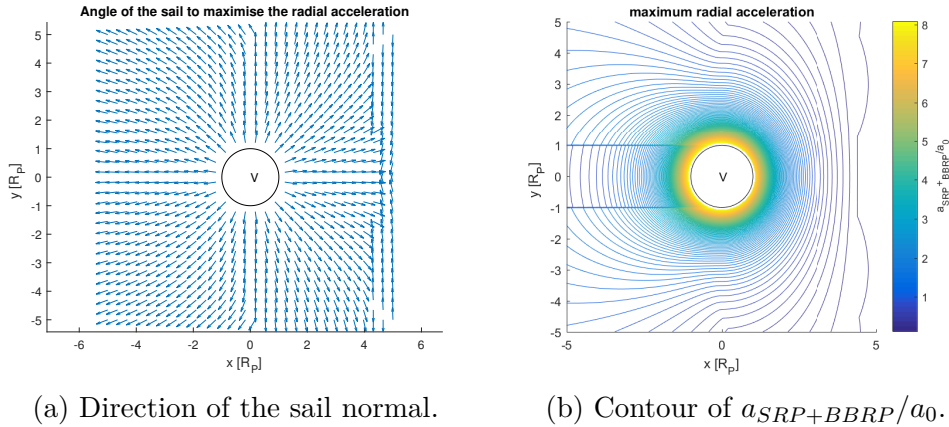


Figure 4.15: Maximisation of radial acceleration, for a single-side coating sail around Venus subject to SRP and BBRP.

When a double-side reflective coating is considered, results can be found in Fig. 4.16. For a maximum radial acceleration, when the sail is placed in points with $x \in [4R_P, 5R_P]$ and $y \in [-1R_P, 1R_P]$, it has a null acceleration to contrast the negative contribution given by the Sun. As regards the direction of the sail normal, Fig. 4.16a shows arrows rotate of 180 deg, specular to the case of SRP only.

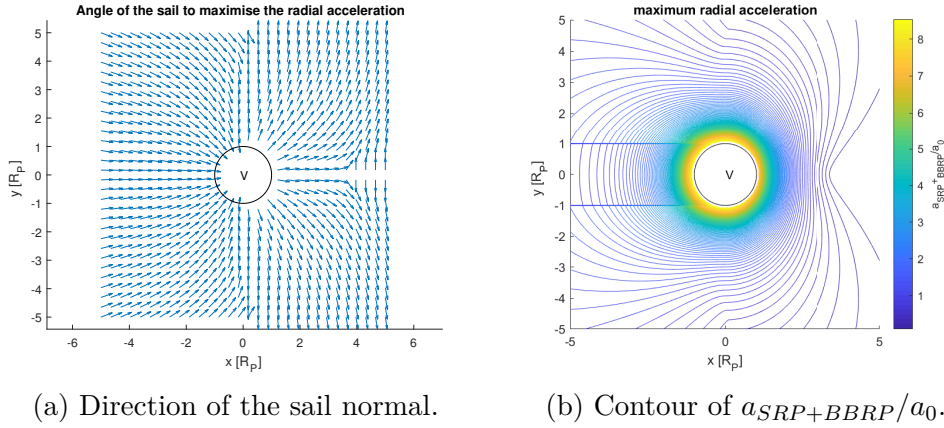


Figure 4.16: Maximisation of radial acceleration, for a double-side coating sail around Venus subject to SRP and BBRP.

4.2.3 SRP+ARP

Albedo occurs only in the daylight part of the planet. For this reason results are found just for half of the grid where the contribution of the ARP can be added. Using the Eq. 2.46 and the parameters show in Table 3.1, it is possible to calculate the ARP and sum it up with the SRP. Results for a planetary sail in the vicinity of Earth and Venus are presented in the next sections.

Earth

For a single-side reflective coating sail (Fig. 4.17) placed close to the Earth, results show that the ARP does not give a great contribution, in fact the graph is not much different from the one in the case with SRP only (Fig. 4.11). A difference occurs just in the region close to the planet, for points with positive x and y in the range $[-0.5R_P, 0.5R_P]$. Adding the ARP the acceleration in this regions turns to a non-zero value and the sail is subjected to the ARP only.

Same results can be obtained with a double-side reflective coating sail as can be seen in Fig. 4.18. There is only one difference in the case of the maximisation of the radial acceleration, in which the region with a null acceleration turns greater than the case of a single-side reflective coating.

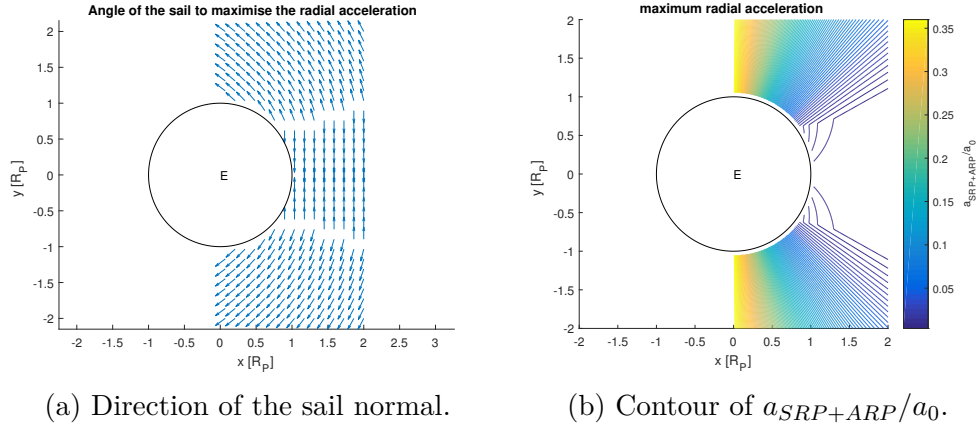


Figure 4.17: Maximisation of radial acceleration, for a single-side coating sail around Earth subject to SRP and ARP.

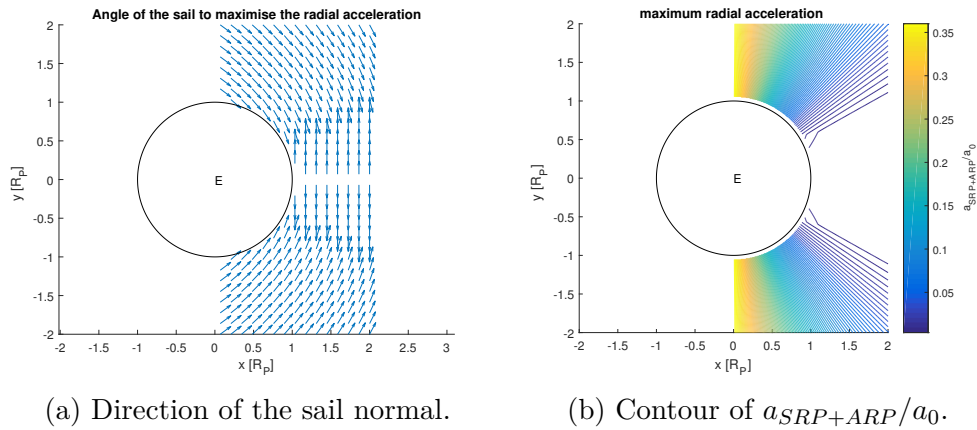


Figure 4.18: Maximisation of radial acceleration, for a double-side coating sail around Earth subject to SRP and ARP.

Venus

In this section the contribution of the albedo on a single- and double-side reflective coating sail in the vicinity of Venus is investigated. As already mentioned, the luminosity due to the albedo is much smaller (two order of magnitude) than the BBRP luminosity. For this reason it has been decided to scale down the grid to $[-2R_P, 2R_P]$. As can be seen from Figs. 4.19 and 4.20, results are similar to the Earth case.

Finally it is possible to state that the albedo does not give a consistent contribution to the behaviour of the sail neither around the Earth, nor around Venus. Nevertheless it has been decided to consider it during the study.

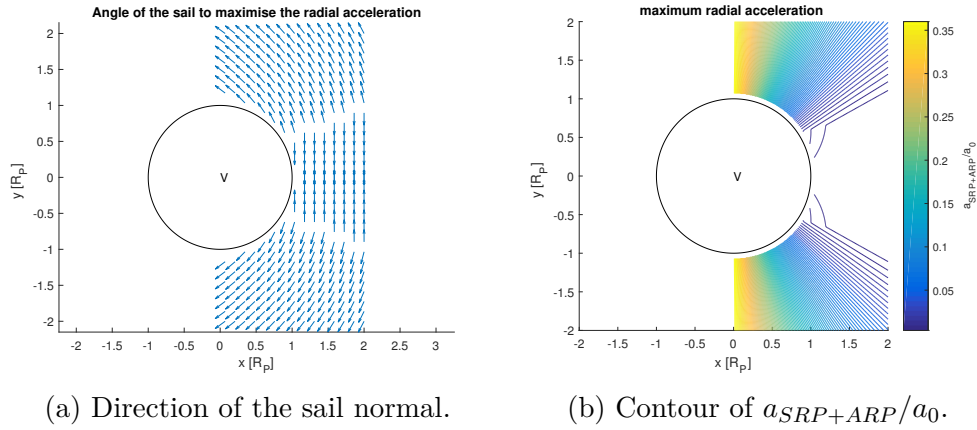


Figure 4.19: Maximisation of radial acceleration, for a single-side coating sail around Venus subject to SRP and ARP.

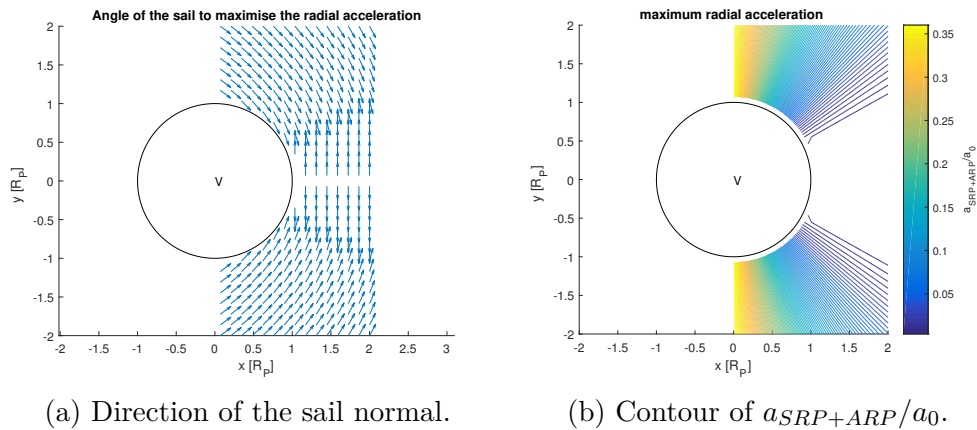


Figure 4.20: Maximisation of radial acceleration, for a double-side coating sail around Venus subject to SRP and ARP.

4.2.4 SRP+PRP

In this section results for the maximization of the radial acceleration are shown for a sail subject to SRP and PRP.

Earth

Fig. 4.21 presents the results for the maximum radial acceleration around the Earth. This can be compared with Fig. 4.11, where the contribution of the SRP is considered. In the eclipse region a great difference can be found. If only SRP is considered,

the radial acceleration cannot be maximised, since no force is exerted on the sail. However, if the contribution of the PRP is taken into account, the sail optimal attitude angle can be found, with the unit normal vector $\hat{\mathbf{n}}$ laying along the radial direction (Fig. 4.21a). As regards the rest of the grid, where the sail is in daylight, the same behaviour is found both considering or not the PRP. However difference occurs when the sail is close to the planet and for positive values of the x . In this region the sail tends to have $\hat{\mathbf{n}}$ along the radial (Fig. 4.21a), and this is due to the effect of the BBRP as can be seen on Fig.4.13a. The contours shown in Figs. 4.21b and 4.11b presents the value of the ratio $a_{SRP+PRP}/a_0$ and a_{SRP}/a_0 , respectively. Out of the eclipse region the trend is similar, with the highest ratio in the left part of the grid, where both SRP and PRP gives a positive contribution to the acceleration. In this region is possible to calculate an increase in the radial acceleration equal to the 9%. Moreover in Fig. 4.21b the gap between the sunlight and eclipse area is underlined by the instantaneous change in the magnitude of the acceleration, switching from maximum to minimum results.

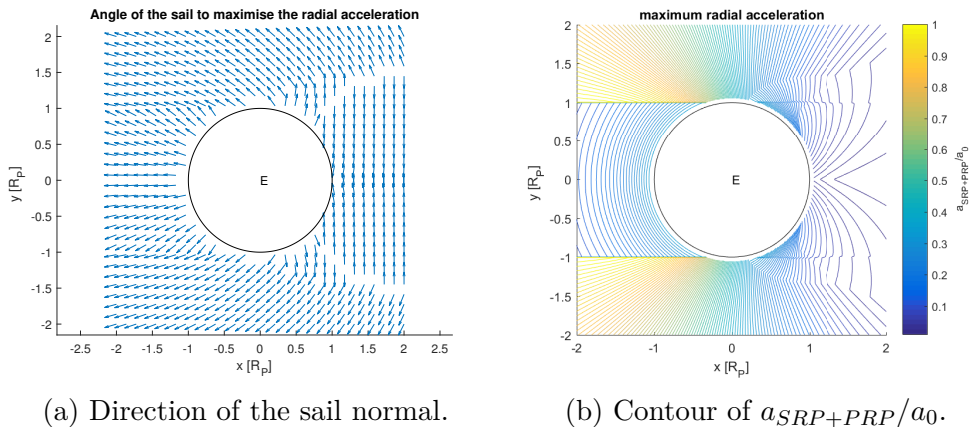


Figure 4.21: Maximisation of radial acceleration, for a single-side coating sail around Earth subject to SRP and PRP.

So far the sail considered has a single-side reflective coating, if this is replaced with a double-side reflective coating the results will change as in Fig. 4.22. Since the symmetry of the problem, the sail will be oriented specular to the single-side case, as can be stated comparing Figs. 4.21a and 4.22a. As regards the radial acceleration, the trend is similar to the single-side case, a change is present for positive x , where the sail, to avoid negative accelerations, is oriented with an attitude angle $\sigma = 90$ or 270 deg, hence with a null acceleration.

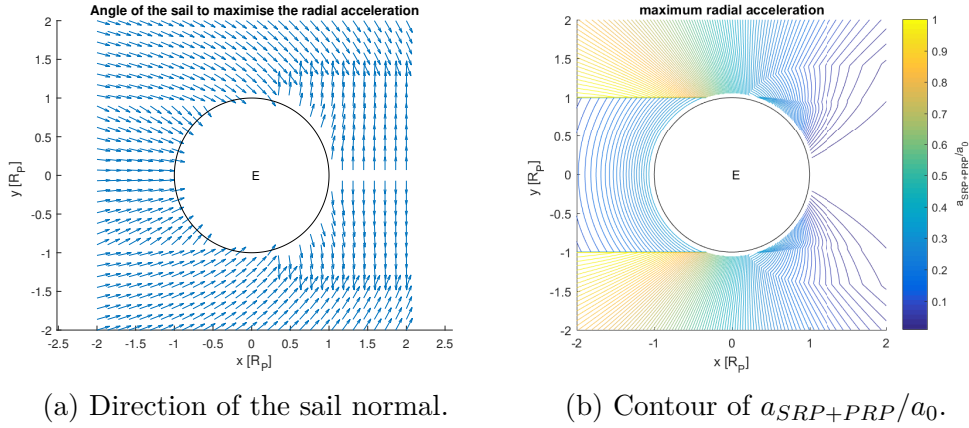


Figure 4.22: Maximisation of radial acceleration, for a double-side coating sail around Earth subject to SRP and PRP.

To summarize the obtained results, four points around the Earth are taken into account:

- Point A= $(-1.9684 \text{ km}, 6.5697 \text{ km})$;
- Point B= $(1.9684 \text{ km}, 6.5697 \text{ km})$;
- Point C= $(-1.9684 \text{ km}, -6.5697 \text{ km})$;
- Point D= $(1.9684 \text{ km}, -6.5697 \text{ km})$;

For these points the ratio of the maximum radial acceleration to the characteristic acceleration and the attitude angle σ that maximises the acceleration in the cases SRP and SRP+PRP are presented in Table 4.2.

Point	$\sigma_{max,SRP}$ rad	$\sigma_{max,SRP+PRP}$ rad	a_{SRP}/a_0	$a_{SRP+PRP}/a_0$	$a_{SRP+PRP}/a_{SRP}$
A	2.3648	1.4277	0.2143	0.3136	1.4635
B	2.6667	2.5095	0.5331	0.67063	1.2579
C	2.6667	2.5095	0.5331	0.67063	1.2579
D	2.3648	1.4277	0.2143	0.3136	1.4635

Table 4.2: Value of the ratio of the maximum radial acceleration to the characteristic acceleration and the attitude angle σ that maximises the acceleration in the cases SRP and SRP+PRP for a sail in the vicinity of the Earth.

It is possible to state that in every point the insertion of the PRP generates an additional contribution, enabling the sail to experience greater acceleration. Moreover in Table 4.2 the values of the optimal σ are present. In the case SRP+PRP

the sail changes its orientation, generating the maximum radial acceleration with lower attitude angle. Points A-D and B-C present the same results thanks to the symmetry of the problem.

Venus

Fig. 4.23 presents the attitude and the ratio $a_{SRP+PRP}/a_0$ in a grid of points around Venus for a single-side reflective coating sail. Since the great contribution given by the PRP, when the sail is close to the planet, it is just oriented along the radial direction (Fig. 4.23a). In this case the consideration of an eclipse region does not causes a difference in the behaviour of the sail since the PRP is the main contribution everywhere. However, when the sail is placed in region with $x > 4R_P$ the behaviour of the sail returns to be similar to the case of SRP only, as can be seen in Fig. 4.12a. The maximum radial acceleration over the specific characteristic acceleration has the trend shown in Fig. 4.23b. The difference with the case SRP only (Fig. 4.12b) is huge, here the highest value of the ratio can be found when the sail is in the region of negative x , while in Fig. 4.23b the closer the sail is to the planet the highest is the ratio, moving from a maximum value of ~ 0.5 (SRP) to ~ 8 when the PRP is taken into account. Moreover the blank region in which the sail was subject to a null radial acceleration is replaced with a higher value of the acceleration.

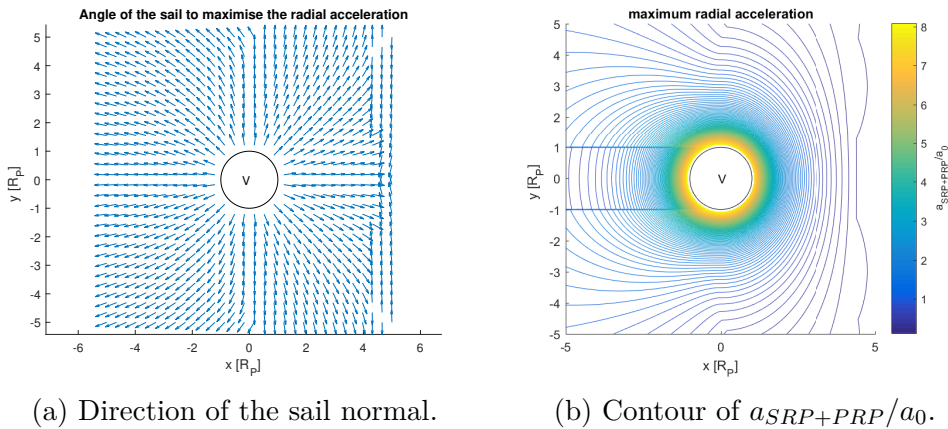


Figure 4.23: Maximisation of radial acceleration, for a single-side coating sail around Venus subject to SRP and PRP.

Same considerations can be done for a double-side reflective coating sail. In this case results for a maximum radial acceleration are shown in Figs. 4.24a and 4.24b. As can be seen, results do not differ from the single-side coating case, what can be underlined is the acceleration of the sail for $x \sim 5$ and $y \sim 0$. The acceleration experienced in that region for a double-side reflective coating sail is smaller than

the one for a single-side case. This is due to the optical characteristics of the back side of the sail where the SRP is exerted and gives a negative contribution.

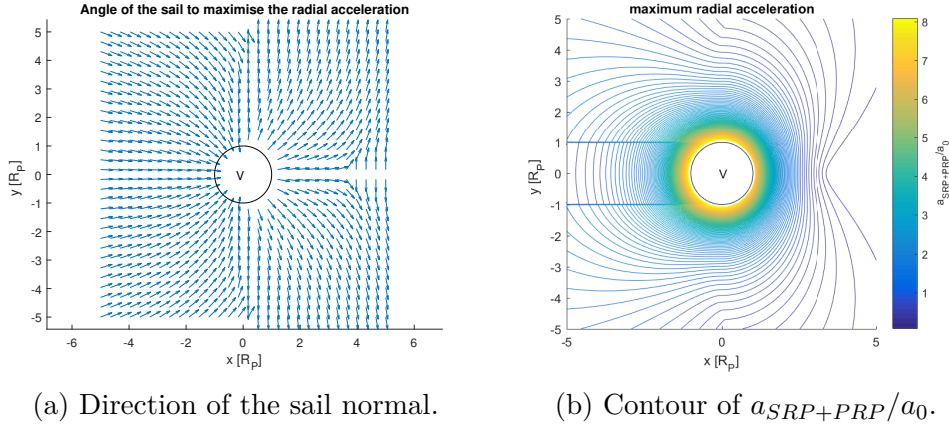


Figure 4.24: Maximisation of radial acceleration, for a double-side coating sail around Venus subject to SRP and PRP.

Considering four points around Venus, it is possible to monitor the behaviour of a single-side reflective coating sail placed in points:

- Point A= $(-1.1556 \text{ km}, 6.7512 \text{ km})$;
- Point B= $(1.1556 \text{ km}, 6.7512 \text{ km})$;
- Point C= $(-1.1556 \text{ km}, -6.7512 \text{ km})$;
- Point D= $(1.1556 \text{ km}, -6.7512 \text{ km})$;

Table 4.3 shows the value of the attitude angle σ that maximises the radial acceleration and the ratio of the acceleration over the characteristic one for the two cases SRP and SRP+PRP.

Point	$\sigma_{max,SRP}$ rad	$\sigma_{max,SRP+PRP}$ rad	a_{SRP}/a_0	$a_{SRP+PRP}/a_0$	$a_{SRP+PRP}/a_{SRP}$
A	2.6101	1.7548	0.2414	7.6299	31.6067
B	2.434	1.4026	0.1434	7.5913	53.049
C	3.8492	4.8806	0.1434	7.5913	53.049
D	3.673	4.5284	0.2414	7.6299	31.6067

Table 4.3: Value of the ratio of the maximum radial acceleration to the characteristic acceleration and the attitude angle σ that maximises the acceleration in the cases SRP and SRP+PRP for a sail in the vicinity of Venus.

The contribution of the PRP enables the sail to experience acceleration up to 50 times greater, obtained with the sail normal laying along the radial direction. Moreover also in this case, as it happened around the Earth, the symmetry of the problem leads to the same results for the points A-C and B-C.

4.3 Maximum transversal acceleration

In this section the transversal acceleration is maximised considering the different contribution due to SRP, BBRP, ARP and the sum of all of them (PRP+SRP).

As already done for the radial acceleration, the same study is conducted for the transversal acceleration of a planetary sail in the vicinity of the Earth and Venus.

4.3.1 SRP

The first studied contribution is the one due to the solar pressure. Results are presented for the two planets and for a sail with a single- and double-side reflective coating.

Earth

In the case of a maximum transverse acceleration for a sail around the Earth, results are shown in Fig. 4.25. Fig. 4.25a presents the direction of the sail normal to maximise the transversal acceleration. In the eclipse region it is impossible to maximise this parameter since no forces is exerted on the sail. As can be seen in Fig. 4.25b, the sail experiences an acceleration equal to zero in the bottom part of the grid for $x \in [-1R_P, 1R_P]$ to contrast the negative contribution of the SRP. In the upper part of the grid the effect of the Sun is positive and the acceleration has a greater magnitude.

Venus

Results for a maximum transverse acceleration around Venus can be found in Fig. 4.26. Results are similar to the case of a sail around the Earth, with greatest acceleration due to the positive contribution of the Sun for positive y while lower value and a region of null acceleration is present for negative y .

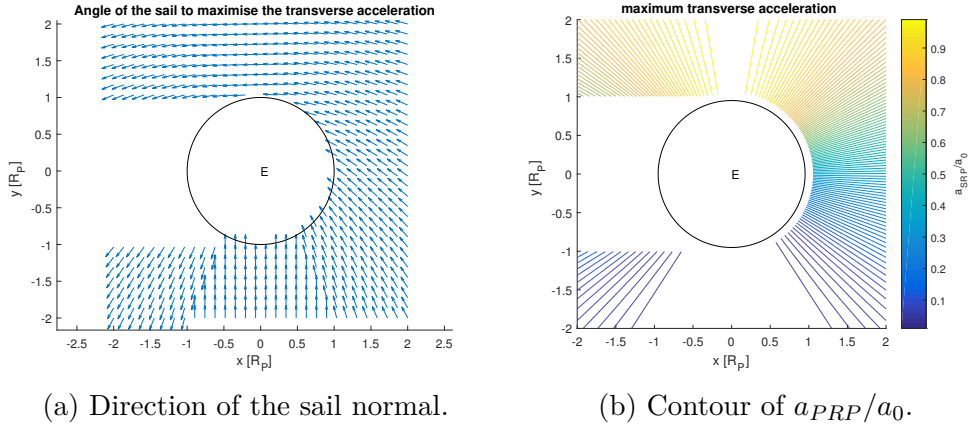


Figure 4.25: Maximisation of transversal acceleration, for a single-side coating sail around Earth subject to SRP.

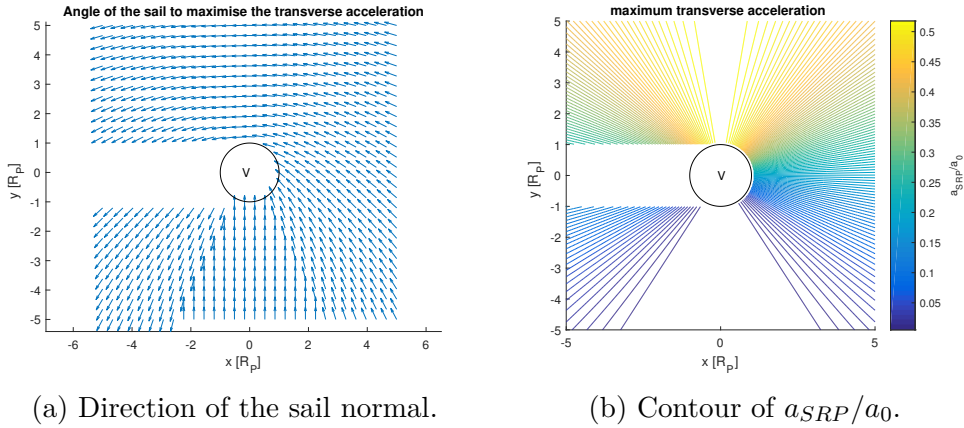


Figure 4.26: Maximisation of transversal acceleration, for a single-side coating sail around Venus subject to SRP.

4.3.2 SRP+BBRP

In this section the contribution of the BBRP is added and the results for different planets will follow.

Earth

For a sail around the Earth, results for the maximum transverse acceleration are presented in Fig. 4.27. Some differences with respect to the case with SRP only (Fig. 4.25) arise:

- the sail is oriented with an angle of ~ 35 deg between the unit normal vector

and the radial direction, as has been analytically found by McInnes [1].

- the sail switches from an attitude angle of 90 to a 270 deg for the points in the bottom part of the grid and with $x \in [-2R_P, -1R_P]$. With this attitude the sail is subject to the force due to the BBRP and the acceleration in this part of the grid presents a non-zero value.

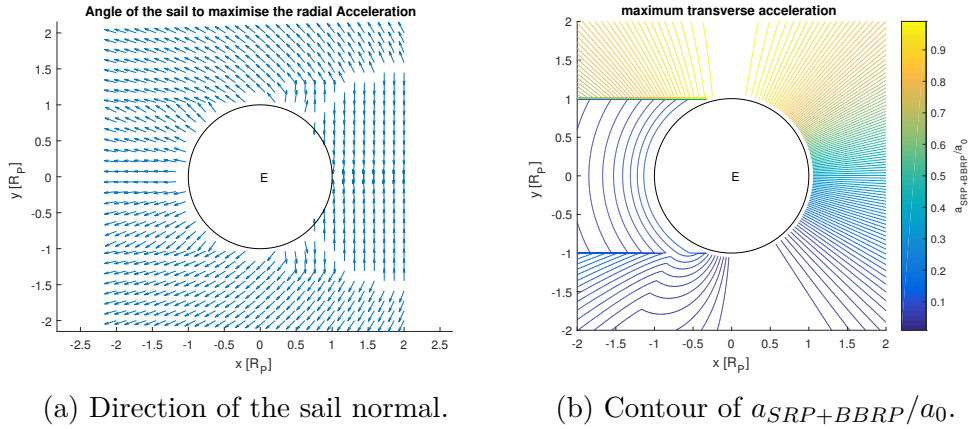


Figure 4.27: Maximisation of transversal acceleration, for a single-side coating sail around Earth subject to SRP and BBRP.

When a double-side reflective coating sail is considered, the obtained results are shown in Fig. 4.28. Comparing them with the case with SRP only, some differences occur especially in the bottom part of the grid for points with negative y and $x \in [0R_P, 0.5R_P]$. In this region in the case SRP only the acceleration is null, it turns into a non-zero when a double-side reflective coating is added, thanks to the contribution of the BBRP.

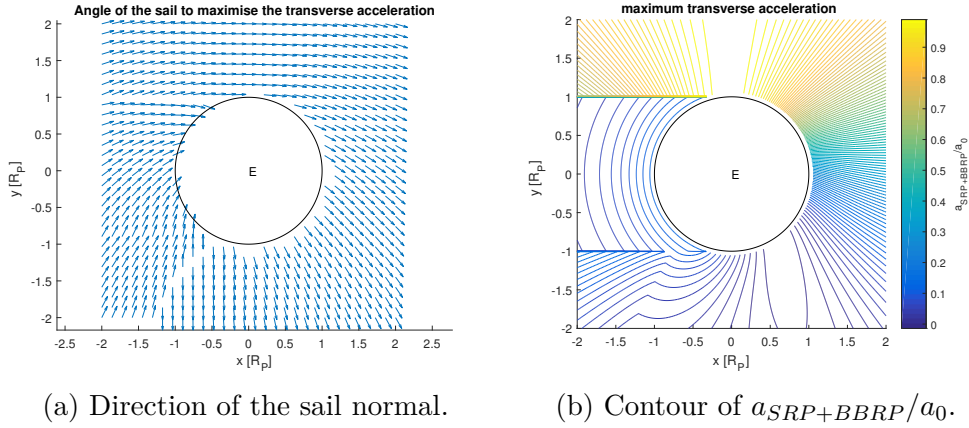


Figure 4.28: Maximisation of transversal acceleration, for a double-side coating sail around Earth subject to SRP and BBRP.

Venus

In this section are presented the results for a sail in the vicinity of Venus with a maximum transversal acceleration.

Fig. 4.29 shows how the insertion of the BBRP leads to results that are different from the case with SRP only:

- For positive x close to the planet, the BBRP is seen as the dominating contribution up to 4 times the radius of Venus.
- For negative x and $y \in [1R_P, 3R_P]$, the sail is oriented differently than in Fig. 4.26 due to the contribution of the BBRP.
- The ratio $a_{SRP+BBRP}/a_0$ is 3.5 times greater than the one obtained for the case SRP only.

As regards the maximum transverse acceleration for a double-side reflective coating sail, the trend in Fig. 4.30a shows a smaller contribution of the BBRP when compared to the case of a single-side reflective coating sail. This can be seen in Fig. 4.30b for negative x and $y \in [3R_P, 4R_P]$ and for positive x and $y \in [0R_P, -5R_P]$.

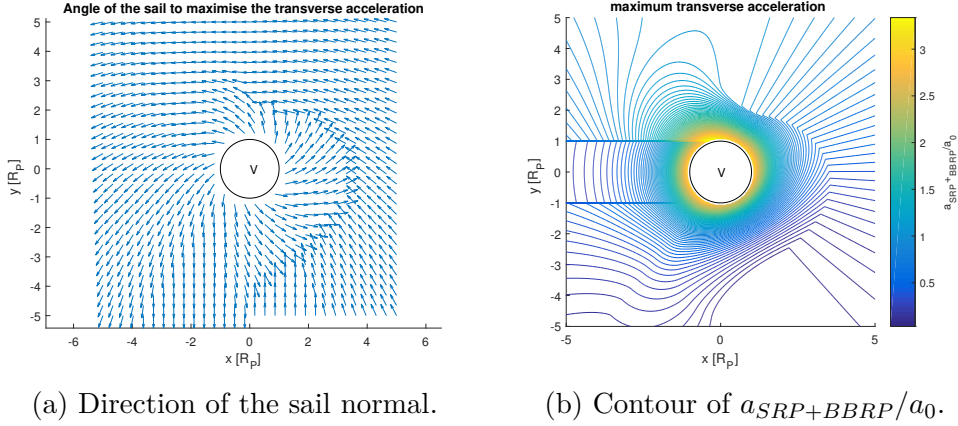


Figure 4.29: Maximisation of transversal acceleration, for a single-side coating sail around Venus subject to SRP and BBRP.

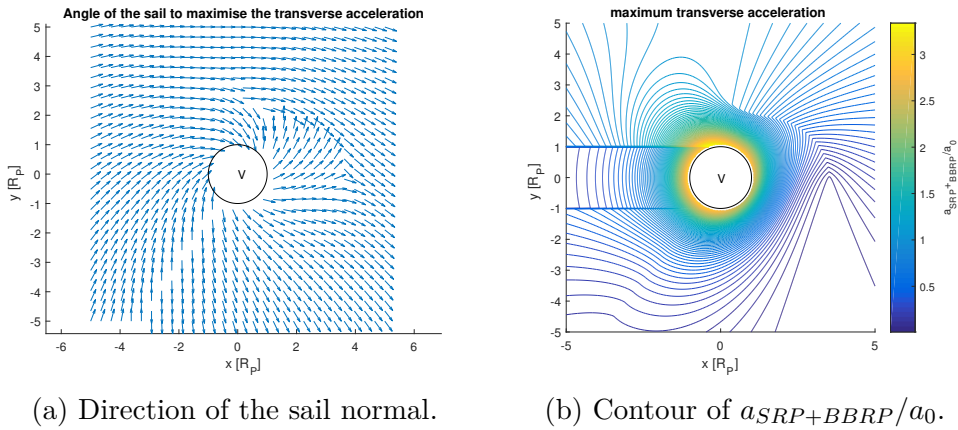


Figure 4.30: Maximisation of transversal acceleration, for a double-side coating sail around Venus subject to SRP and BBRP.

4.3.3 SRP+ARP

As already mention in the case maximum radial acceleration, albedo has a small luminosity and it occurs just in the daylight part of the planet.

Earth

For a single-side reflective coating sail around the Earth (Fig. 4.31), results show that the ARP does not give a great contribution, in fact the graphs are not much different from the one in the case with SRP only (Fig. 4.25). Same results can be obtained with a double-side reflective coating sail as can be seen in Fig. 4.32.

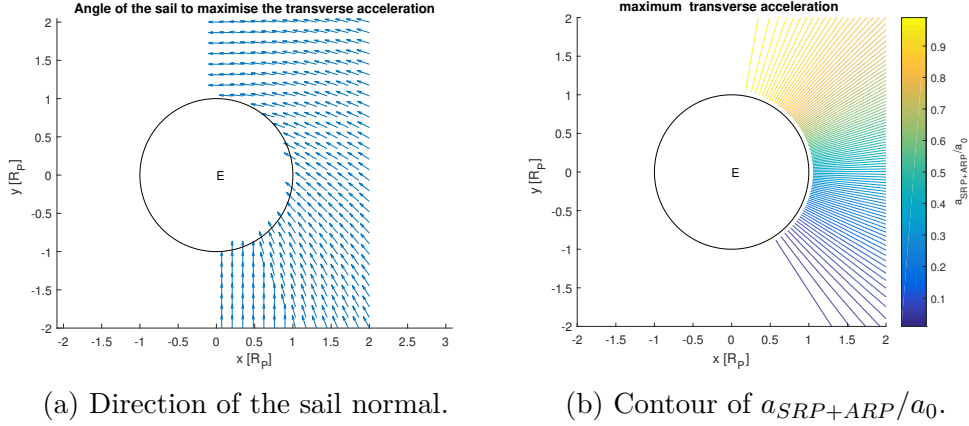


Figure 4.31: Maximisation of transversal acceleration, for a single-side coating sail around Earth subject to SRP and ARP.

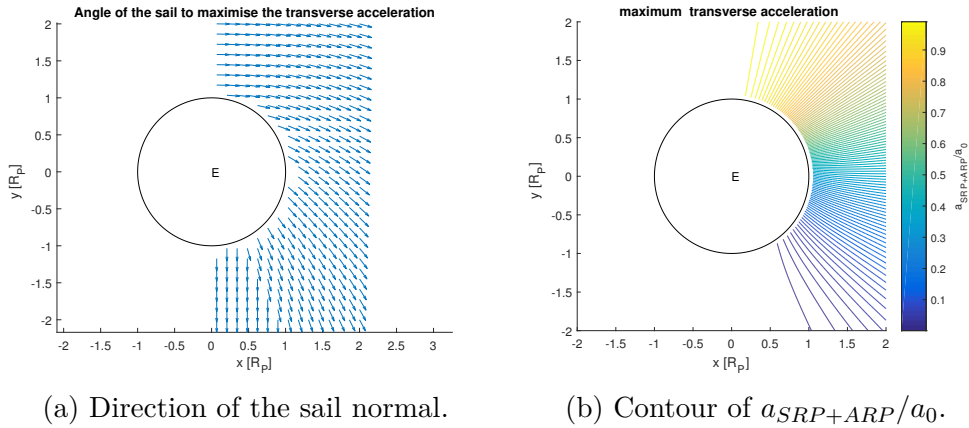


Figure 4.32: Maximisation of transversal acceleration, for a double-side coating sail around Venus subject to SRP and ARP.

The analysis of these results shows that the contribution of the albedo around the Earth is not great. However, for completeness, it is taken into account during the entire work.

Venus

Considering a sail in the vicinity of Venus, subject to SRP and ARP leads to results shown in Fig. 4.33. Also in this case it has been decided to use a smaller grid since the contribution due to the albedo is small. Results are similar to the case of a sail around the Earth both for a single- and a double-side reflective coating. For this they are not deeply investigated.

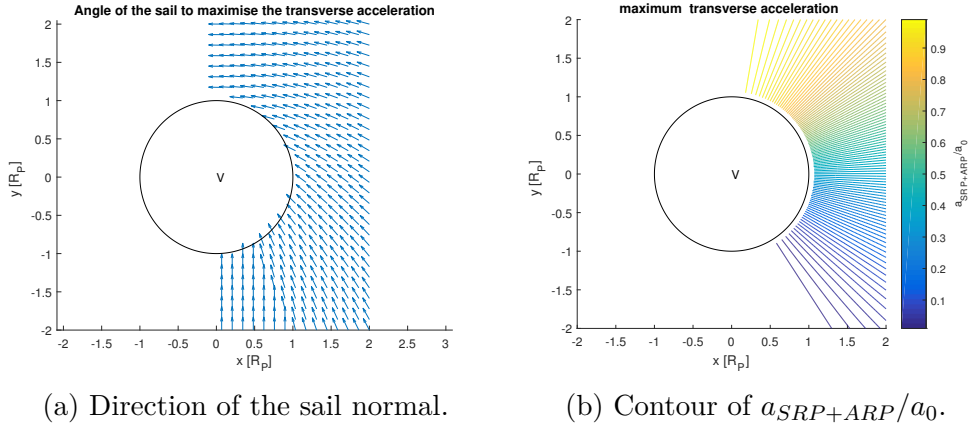


Figure 4.33: Maximisation of transversal acceleration, for a single-side coating sail around Venus subject to SRP and ARP.

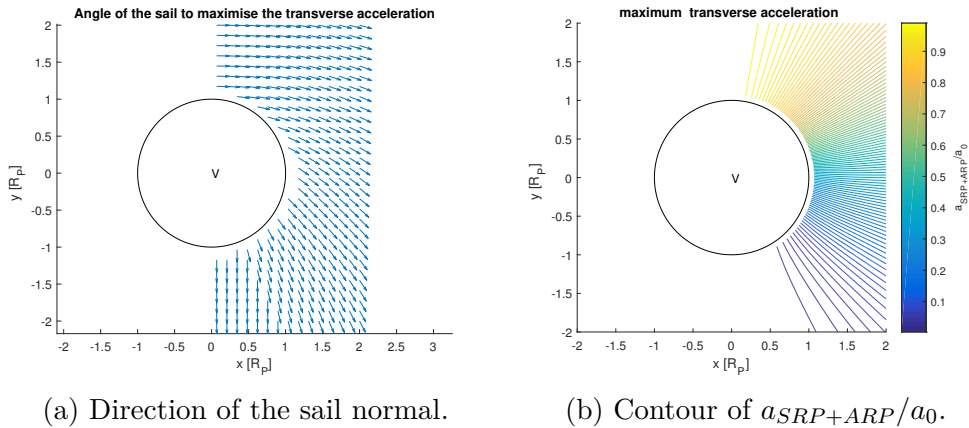


Figure 4.34: Maximisation of transversal acceleration, for a double-side coating sail around Venus subject to SRP and ARP.

4.3.4 SRP+PRP

In this last section the contributions of the BBRP and ARP are summed up together with the SRP.

Earth

The maximization of the acceleration along the transverse direction for a sail around the Earth, leads to the results in Figs. 4.35 and 4.25 considering SRP+PRP and SRP only, respectively. In this case the PRP causes a configuration of the sail that creates an angle $\delta \sim 35$ deg in the eclipse region. As already mentioned, this

results can be confirmed by the analytical study conducted by McInnes [1], where the author shows that a sail subject to a radial radiation will be oriented at an angle equal to 35.26 deg if the transverse acceleration has to be maximised. Out of the umbra region, the cases of SRP only and SRP+PRP present different orientation of the sail. When it is placed in the points with negative y and x near 0 the SRP gives a negative contribution to the transverse acceleration, for this reason the sail is oriented with a pitch angle equal to 90 deg that leads to a null acceleration (Fig. 4.25b). Adding the PRP, the sail experiences a sudden change of attitude in the point around $x = 0$. This is due to the fact that for negative x , PRP gives a positive contribution to the acceleration while for positive x the contribution is negative. This can also be visualized in the Figs. 4.35b and 4.25b, where in the case SRP only the sail has a null acceleration and it becomes positive when the PRP is added.

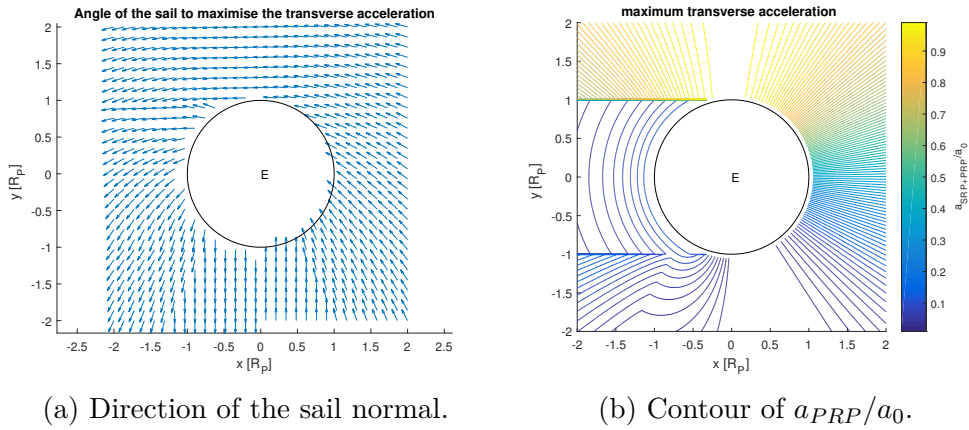


Figure 4.35: Maximisation of transversal acceleration, for a single-side coating sail around Earth subject to SRP and PRP.

When a double-side reflective coating sail is considered, results can be found in Fig. 4.36. In this case there is not a great difference with a single-side reflective coating sail. What changes is the acceleration experienced by the sail in the in the lower part of the grid, as can be seen in Fig. 4.36b, where the use of a double-side reflective coating sail enables to reduce the region of null acceleration.

As already done for the maximum radial direction, also in this case the same four points around the Earth are taken into account and their results are presented in Table 4.4.

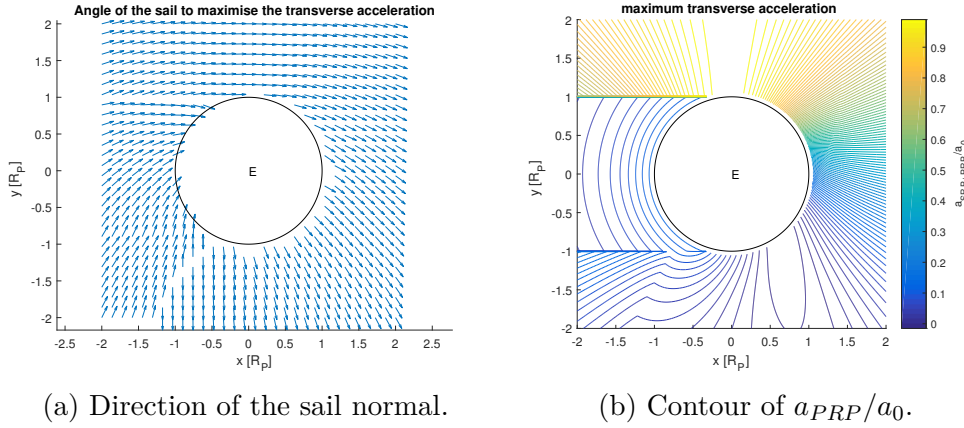


Figure 4.36: Maximisation of transversal acceleration, for a double-side coating sail around Earth subject to SRP and PRP.

Point	$\sigma_{max,SRP}$ rad	$\sigma_{max,SRP+PRP}$ rad	a_{SRP}/a_0	$a_{SRP+PRP}/a_0$	$a_{SRP+PRP}/a_{SRP}$
A	3.2391	3.1888	0.9715	0.9851	1.0141
B	3.0441	3.0441	0.9715	0.9715	1
C	1.5724	4.7108	0	0.079	∞
D	1.5724	1.5724	0	0	

Table 4.4: Value of the ratio of the maximum transversal acceleration to the characteristic acceleration and the attitude angle σ that maximises the acceleration in the cases SRP and SRP+PRP for a sail in the vicinity of the Earth.

From these results is possible to state that the addition of the PRP for the maximisation of the transversal does not give a much great contribution especially for positive x . This is not true if point C is considered. In fact, in this case the gain is infinite since the sail pass from a null acceleration to a positive one. Since the contribution is not great, there is also no difference in the orientation of the sail for points B and D, while in A and C the sail changes the attitude angle when the radiation coming from the planet is considered.

These results show that PRP could give a contribution to the dynamics of the sail, however it is better to implement a real-case scenario, such as a manoeuvre around the planet, to quantify the actual contribution of the PRP coming from the Earth.

Venus

The case of a maximum transverse acceleration for a sail around Venus leads to the results shown in Figs. 4.37 and 4.26 for the case SRP+PRP and PRP only, respectively. The optimal attitude of the sail, considering the radiation emitted by Venus, is presented in Fig. 4.37a. Comparing these results with the ones in Fig. 4.26a, it is possible to identify a great difference in the attitude of the sail. In fact, for positive y in the range $[0R_P, 2R_P]$ the sail is no more oriented with an attitude angle $\sigma = 180$ deg. The contribution is even bigger in the case of positive x , where the sail switches from facing the Sun in the case fo SRP only, to facing the planet, when the PRP is added. In this case the highest value of the ratio is decreased to 3.5, but it is still possible to state that adding the PRP the sail experienced a much greater acceleration than in the case of SRP only. What stays the same between the two case, even if for different magnitude, is that for positive large value of y , the sail experienced the highest acceleration thanks to the contribution given by the Sun. Another results that can be underlined, in the case of SRP+PRP, is that when the sail is close to the planet, in the region with positive y and negative x , the acceleration is greater than in the case of negative y and positive x . This is caused by the PRP, in fact it gives an additional contribution in the first region and a negative contribution for the latter one.

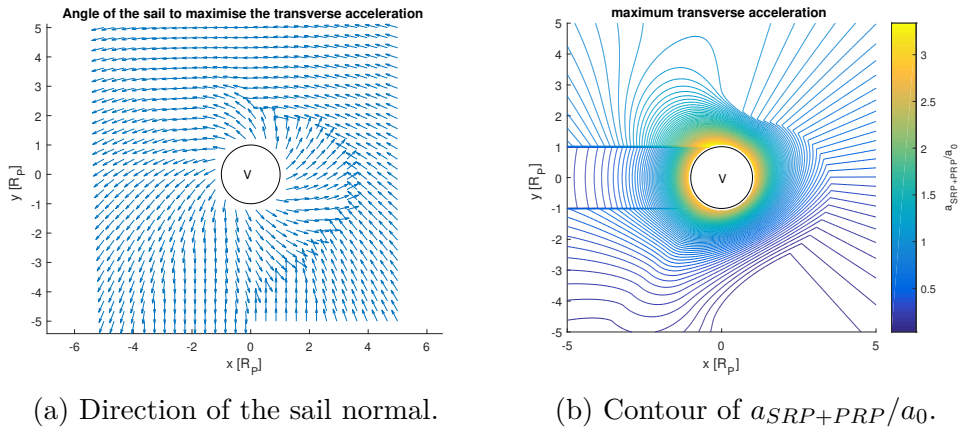


Figure 4.37: Maximisation of transversal acceleration, for a single-side coating sail around Venus subject to SRP and PRP.

The case of a maximum transverse acceleration for a double-side reflective coating is presented in Figs. 4.38a and 4.38b. The main contribution is still the PRP, but the main difference with the case of a single-side sail can be found for $y < 0$, where the negative contribution coming from the Sun is more experienced because of the reflection coefficient of the back side of the sail.

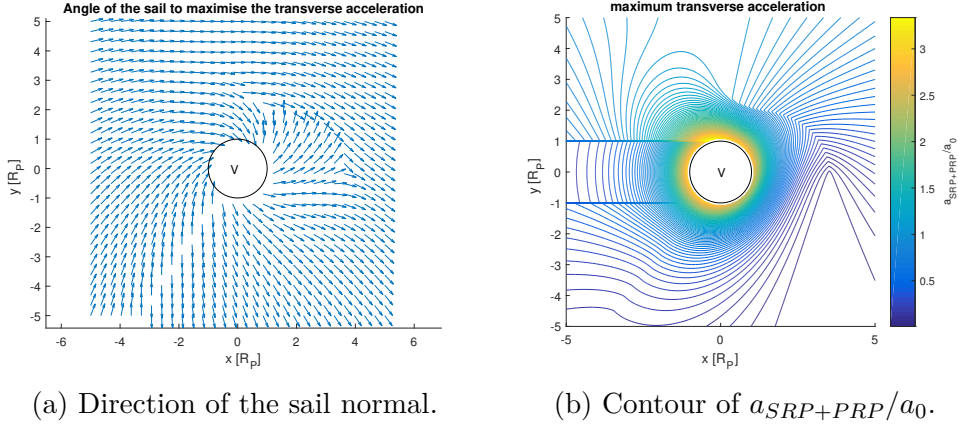


Figure 4.38: Maximisation of transversal acceleration, for a double-side coating sail around Venus subject to SRP and PRP.

Table 4.5 presents the results for the same four points used in the case maximum radial acceleration:

- Point A= $(-1.1556 \text{ km}, 6.7512 \text{ km})$;
- Point B= $(1.1556 \text{ km}, 6.7512 \text{ km})$;
- Point C= $(-1.1556 \text{ km}, -6.7512 \text{ km})$;
- Point D= $(1.1556 \text{ km}, -6.7512 \text{ km})$;

Point	$\sigma_{max,SRP}$ rad	$\sigma_{max,SRP+PRP}$ rad	a_{SRP}/a_0	$a_{SRP+PRP}/a_0$	$a_{SRP+PRP}/a_{SRP}$
A	3.1951	2.4214	0.5176	3.1118	6.012
B	3.0881	2.0567	0.5176	2.9122	5.6264
C	1.5724	5.4718	0	2.4127	∞
D	1.5724	5.4718	0	2.5537	∞

Table 4.5: Value of the ratio of the maximum transversal acceleration to the characteristic acceleration and the attitude angle σ that maximises the acceleration in the cases SRP and SRP+PRP for a sail in the vicinity of Venus.

The contribution of the PRP around Venus leads to an improvement of the sail performances in each of the four points. Moreover for negative y the sail has a no-zero value when the PRP is added, with an infinite gain of the acceleration. As regards the attitude angle σ it changes in the two cases, since when the PRP is added it becomes the dominating contribution.

After analysing all these results, it is possible to state that the PRP in the case of a sail around Venus, is the main contribution of the acceleration. In particular the BBRP is by far the dominating contribution, while the albedo does not give a great effect on results.

In the next chapter, using the same methodology applied in this section, is to integrate a manoeuvre around the Earth and Venus, trying to quantify the contribution of the PRP in a real-case scenario.

Chapter 5

Control law for semi-major axis increase

Knowing the acceleration of a sail in a grid of points around a celestial body, a real-case scenario can be considered, placing the sail in orbit around a planet. The study considers a semi-major axis increasing manoeuvre to evaluate the percentage increase obtained when the PRP is considered. Results around Earth and Venus are shown for a sail with a characteristic acceleration equal to 1 mm/s^2 and the cases of SRP only and SRP+PRP are analysed.

To evaluate the variation of the orbital elements, Gauss' form of the Lagrange variational equations is used. In this case the acceleration vector \mathbf{a} is written in components taken in the rotating frame $\{\mathbf{v}, \mathbf{n}^*, \mathbf{h}\}$. In this frame the direction vector \mathbf{v} is along the orbit velocity vector, \mathbf{n}^* is the normal direction to the velocity, where the dash has been added not to create confusion with the normal direction of the sail $\hat{\mathbf{n}}$, and \mathbf{h} is the out of plane component.

Gauss' variational equation can be written as [24]

$$\frac{da}{dt} = \frac{2a^2v}{\mu} a_v \quad (5.1)$$

$$\frac{de}{dt} = \frac{1}{v} \left[2(e + \cos f) a_v - \frac{r}{a} \sin f a_{n^*} \right] \quad (5.2)$$

$$\frac{di}{dt} = \frac{r \cos \theta}{h} a_h \quad (5.3)$$

$$\frac{d\Omega}{dt} = \frac{r \sin \theta}{h \sin i} a_h \quad (5.4)$$

$$\frac{d\omega}{dt} = \frac{1}{ev} \left[2 \sin f a_v + \left(2e + \frac{r}{a} \cos f \right) a_{n^*} \right] - \frac{r \sin \theta \cos i}{h \sin i} a_h \quad (5.5)$$

$$\frac{df}{dt} = \frac{h}{r^2} - \frac{1}{ev} \left[2 \sin f a_v + \left(2e + \frac{r}{a} \cos f \right) a_{n^*} \right] \quad (5.6)$$

Where:

- a is the semi-major axis;
- e is the eccentricity;
- i is the inclination
- Ω is the right ascension of the ascending node (RAAN);
- ω is the argument of periapsis;
- f is the true anomaly;
- $\theta = \omega + f$;
- $v = \sqrt{\mu \left(\frac{2}{r} - \frac{1}{a} \right)}$.

As this work is two dimensional, so the out of plane acceleration will not be considered ($\mathbf{a}_h = 0$). Hence there is no variation of Ω , i and also the last term in Eq. 5.5 is null.

This study considers a planar initial orbit in the ecliptic plane with an high eccentricity, a low periapsis and various positions of the argument of the periapsis. The trajectories with $\omega = 0, 90, 180, 270$ deg are denominated T1, T2, T3 and T4, respectively. Table 5.1 presents the values of the orbital elements of the starting orbit.

To change the semi-major axis the most efficient strategy is to use a tangential control law. The variation of the semi-major axis (a) reaches maximum value at the periapsis since the velocity magnitude is the largest in that point [25]. For this reason, it has been decided to use a control law that maximises the acceleration in the direction of the velocity when the sail is in a periapsis-centred arc of ± 30 deg (Fig. 5.1). This control law does not lead to an optimal solution, but since the aim of this work is to compare the results in the cases SRP and SRP+PRP, it is not necessary to use the optimal one, what matters is that the same control law is used in both cases.

In the next sections the results of the integration of sail control law, for four orbits are shown (in terms of trajectory, acceleration and semi-major axis) for Earth and Venus. Different arguments of periapsis with respect to the Sun direction will be studied, trying to investigate how the inclusion of the PRP changes the results.

Semimajor axis a [km]	Eccentricity e	Inclination i [deg]	RAAN Ω [deg]	Argument of periapsis ω [deg]	True anomaly f [deg]
36840	0.8	0	0	0, 90, 180, 270	0

Table 5.1: Orbital elements

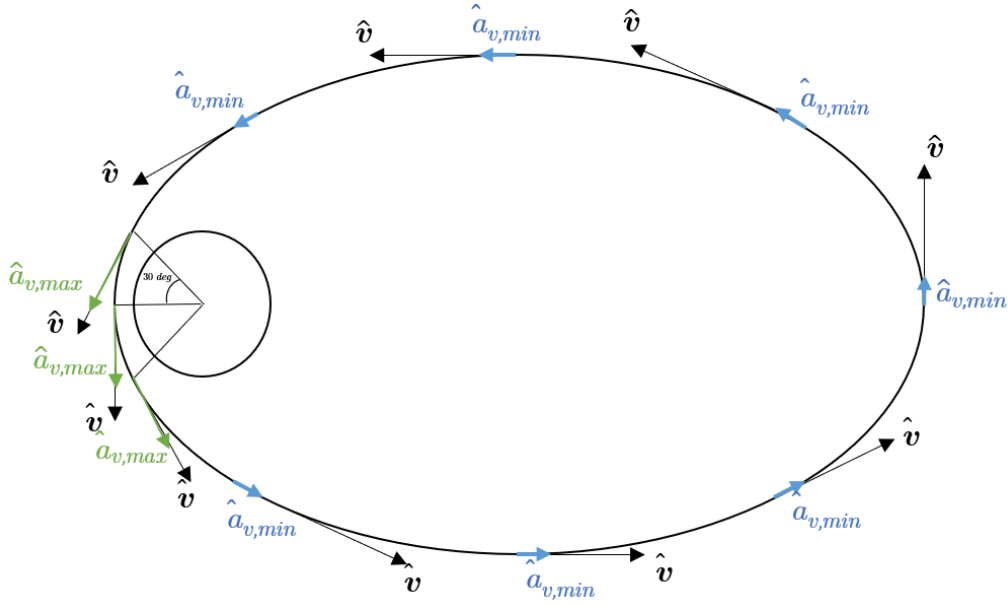


Figure 5.1: Control law

5.1 Earth

The first case considers the sail orbiting around the Earth with an argument of periapsis $\omega = 0$ deg. Fig. 5.2 shows the trajectory over time and the orientation of the sail to obtain the desired acceleration. The increment of the semi-major axis (a) is not substantial, but using Fig. 5.3a it is possible to compare the trend in the case of SRP only and SRP+PRP. It increases with time: with SRP only one has a step increase corresponding to the arc. Thanks to the PRP the trend is shifted up and it is not a precisely step increase. This is due to the fact that adding the PRP the sail experiences a non-zero acceleration for time equal to $0.7 \cdot 10^5$ s and $1.4 \cdot 10^5$ s, as can be seen in Fig. 5.3b. Fig. 5.3c shows the behaviour of the acceleration along the velocity when the sail is around the pericentre. It is possible to express a percentage increase of the semi-major axis considering the variation of a from the start time to the final time, in the case SRP and SRP+PRP (Fig. 5.3a). In this case, the increase is of 19.89%.

Analysing the acceleration of the sail along the velocity, Fig. 5.3c presents a trend quite similar between the two cases. As already mentioned, a difference can be found at the beginning and at the end of every orbit. In fact, in this range the PRP leads to an acceleration that is not null. This happens because in most of the trajectory the minimum acceleration is required and the sail is oriented with $\sigma = 90$ or 270 deg to ensure a null acceleration. When the sail gets closer to the periapsis the contribution

of the PRP is greater and the minimum acceleration is not zero any more.

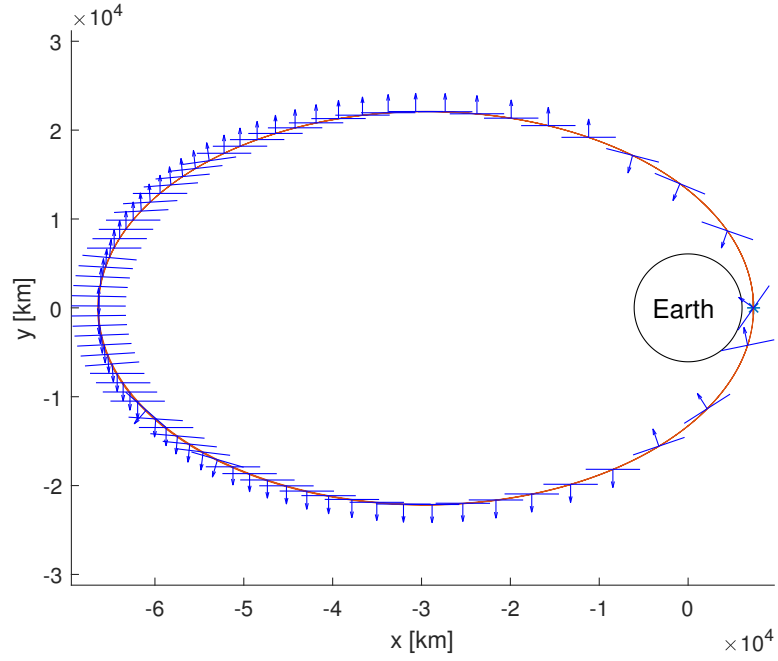
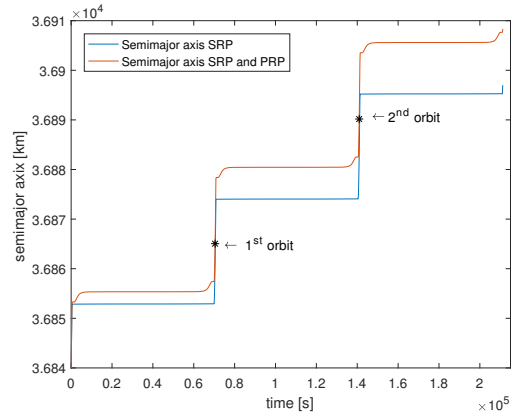
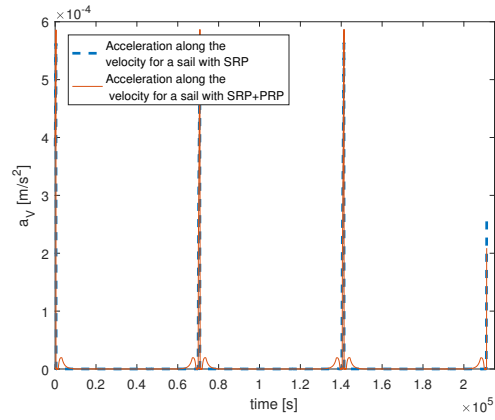


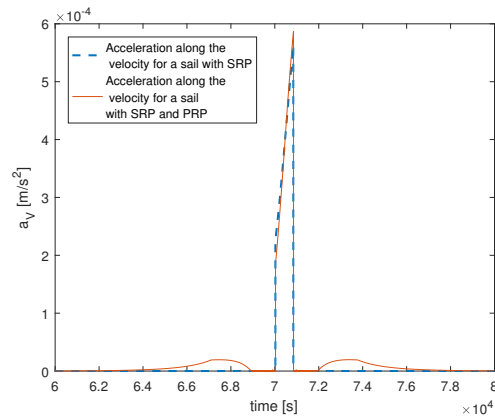
Figure 5.2: Trajectory around the Earth with orientation of the sail with $\omega = 0$ deg



(a) Semi-major axis with SRP and SRP+PRP.



(b) Acceleration along the velocity for a sail with SRP and SRP+PRP.



(c) Acceleration along the velocity around the pericentre.

Figure 5.3: Results for a sail around the Earth with $\omega = 0$ deg.

The second case considers $\omega = 90$ deg. The trajectory with the orientation of the sail is presented in Fig. 5.4, here it is possible to identify points with a sudden change of the attitude angle. For example from the 11th to the 24th point the minimum acceleration can be found for an angle $\sigma \simeq 1.5$ rad. Then if the 25th point is considered, σ switches to value of 4.72 rad. To explain this behaviour points A (24th) and B (25th) are taken into account and the value of the acceleration along the velocity direction is presented in function of the attitude angle σ . Fig. 5.5 shows how the sail experiences a minimum positive acceleration for different values of σ . For point A the first minimum value is taken as the optimal attitude, while point B considers the third minimum as the optimal one. This behaviour is due to the discretization of the attitude angle: since it is not possible to find the exact zero, the code select the closest value. This can be found in proximity of the roots of the function and it is not possible to pick the value with smaller σ .

As can be seen in Fig. 5.6, the presence of the PRP gives a small positive contribution to the dynamics of the sail. After three orbits the semi-major axis has reached the 1.84% of increment. Fig. 5.6b shows the trend of the acceleration along the trajectory, while Fig. 5.6c presents the trend of a_V around the pericentre. No consistent difference is present, with the Sun always being the dominating contribution in both cases.

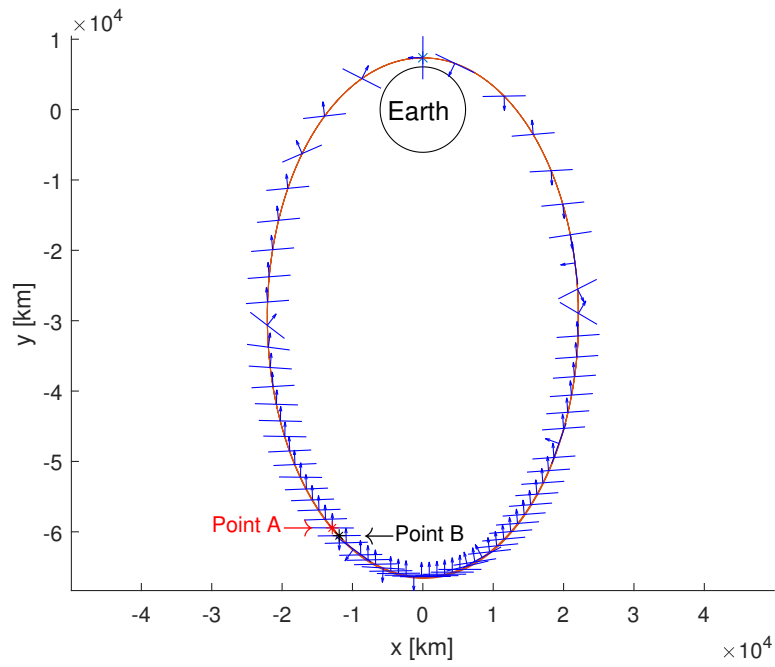


Figure 5.4: Trajectory around the Earth with orientation of the sail with $\omega = 90$ deg

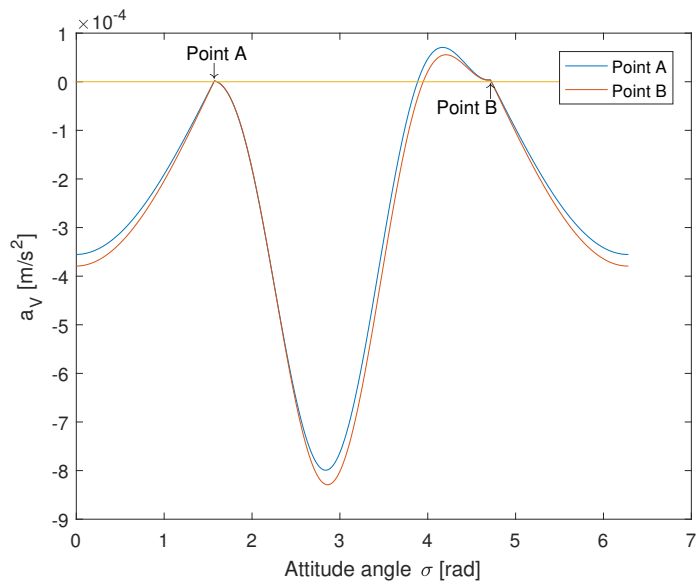
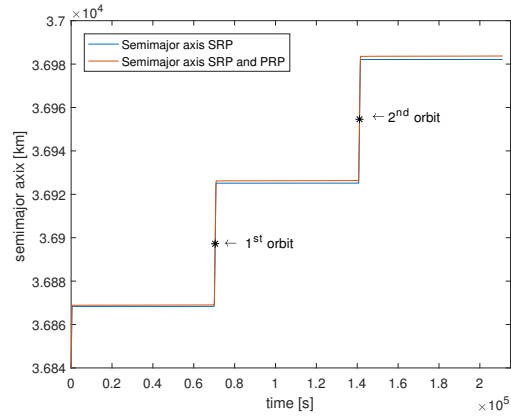
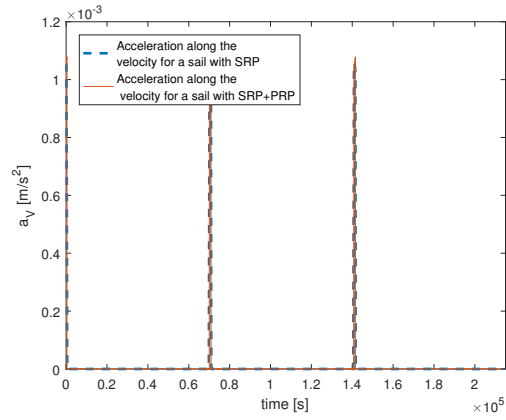


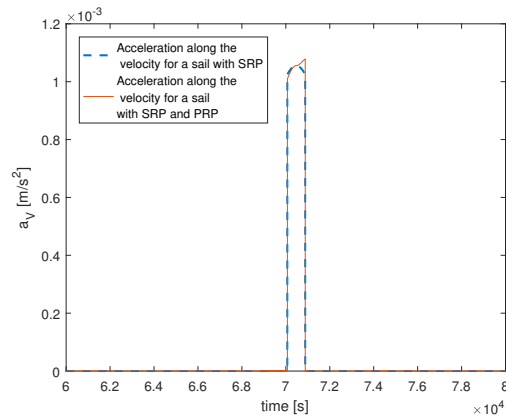
Figure 5.5: Trend of the acceleration along the velocity in function of the attitude angle, for point A and B



(a) Semimajor axis with SRP and SRP+PRP.



(b) Acceleration along the velocity for a sail with SRP and SRP+PRP.



(c) Acceleration along the velocity around the pericentre.

Figure 5.6: Results for a sail around the Earth with $\omega = 90$ deg.

The study has proceeded considering an orbit with the periapsis in the eclipse region, hence $\omega = 180$ deg. As can be seen from Fig. 5.7, the arc mostly lays in the shadow region. For this reason when only the SRP is considered the variation of the semi-major is near zero. Results change adding the PRP, with a step increase of a (Fig. 5.8a). In this case the calculated percentage increase is almost infinite. As regards the acceleration, Figs. 5.8b and 5.8c show how the sail has an almost null acceleration throughout the orbit when the SRP is considered and a non-zero one thanks to the contribution of the PRP. These results show how considering the PRP a semi-major axis increase is possible even if the periapsis is in the eclipse region.

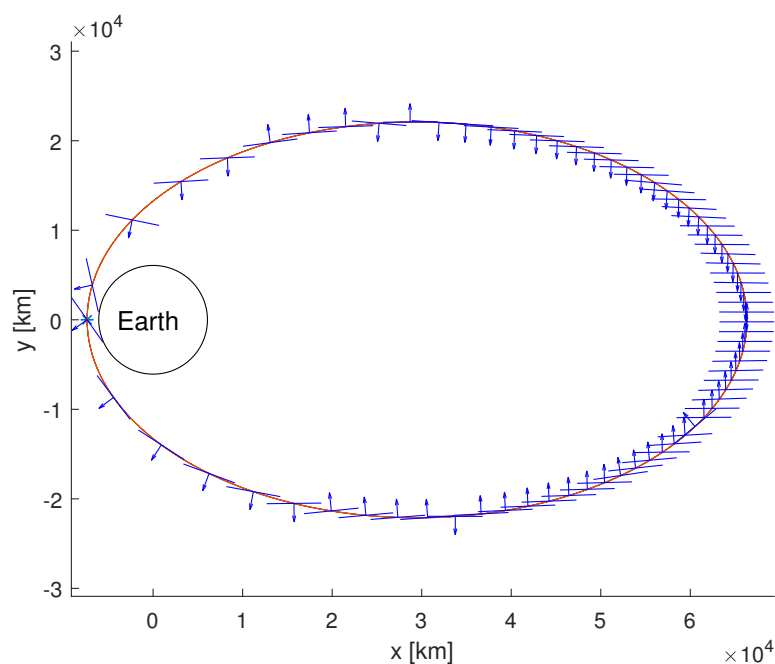
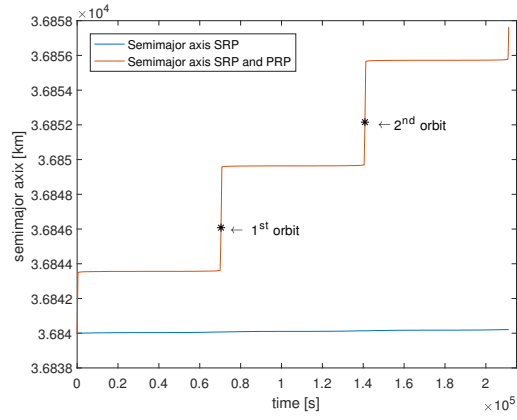
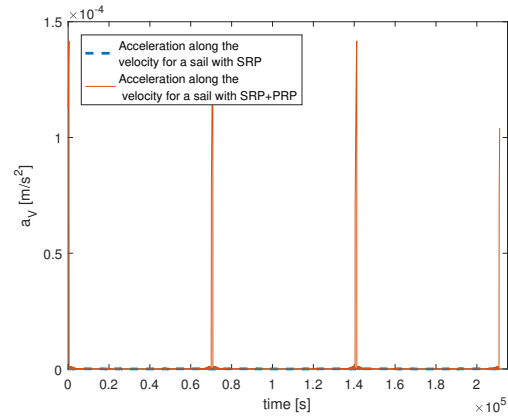


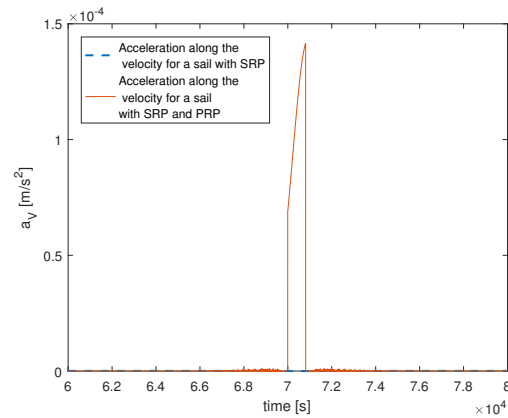
Figure 5.7: Trajectory around the Earth with orientation of the sail with $\omega = 180$ deg



(a) Semimajor axis with SRP and SRP+PRP.



(b) Acceleration along the velocity for a sail with SRP and SRP+PRP.



(c) Acceleration along the velocity around the pericentre.

Figure 5.8: Results for a sail around the Earth with $\omega = 180$ deg.

In the last case the argument of periapsis is placed at 270 deg and the arc is in a region where the Sun gives a negative contribution. For this reason, also in this case the variation of the semi-major axis is small considering the SRP only (Fig. 5.10a). When the PRP is added, the results show a different trend and this lead to have an increase of the $\sim 7000\%$ of the semi-major axis. However case SRP+PRP does not have a step trend since throughout the trajectory the sail is oriented with an angle $\sigma \simeq 90$ or 270 deg and only the contribution of the planet is considered. This leads to the presence of small peaks of acceleration in Fig. 5.10b, with the sail thrusting slightly also outside of the arc. Fig. 5.10c shows the trend of the acceleration around the pericentre. When the sail is placed at the pericentre with $f = 0$ it experiences a null acceleration since the Sun gives a negative contribution that cannot be counteracted by the PRP.

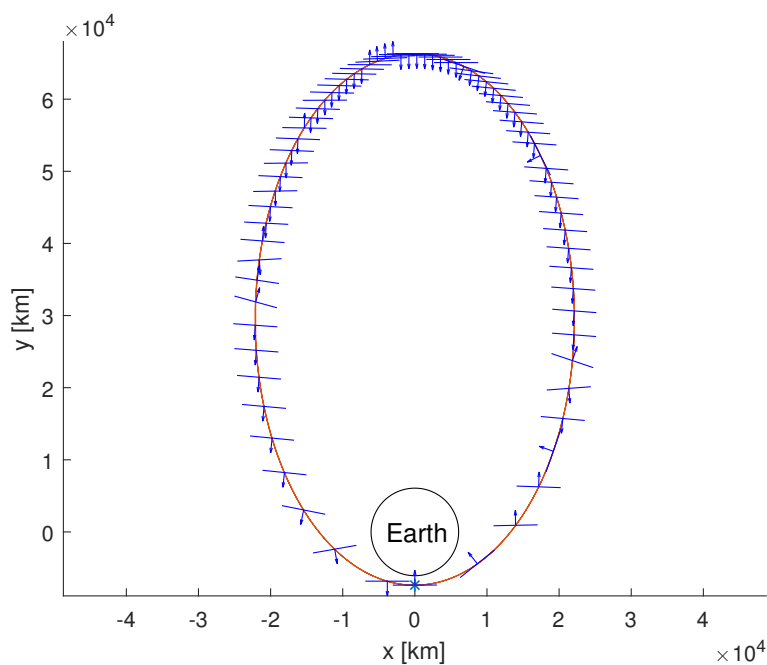
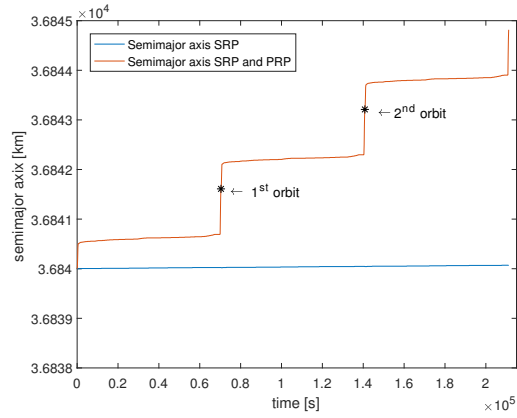
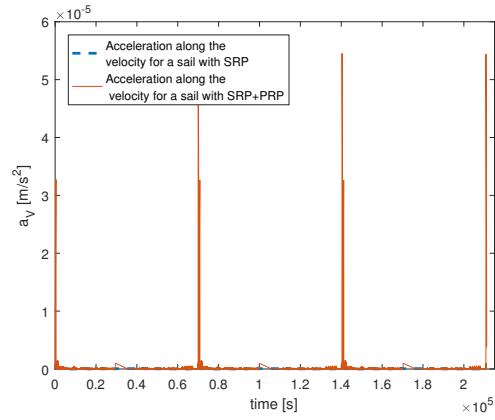


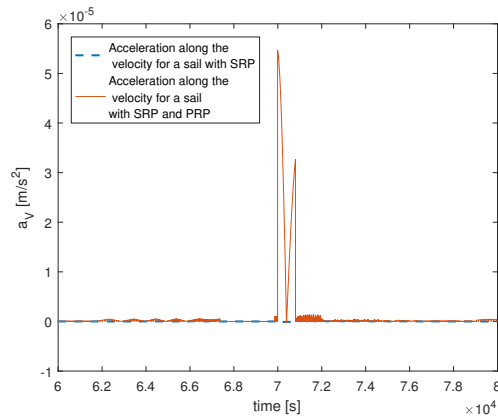
Figure 5.9: Trajectory around the Earth with orientation of the sail with $\omega = 270$ deg



(a) Semimajor axis with SRP and SRP+PRP.



(b) Acceleration along the velocity for a sail with SRP and SRP+PRP.



(c) Acceleration along the velocity around the pericentre.

Figure 5.10: Results for a sail around the Earth with $\omega = 270$ deg.

Trajectory	Increase with SRP+PRP	Increase with SRP	Absolute percentage increase
T1	0.1547%	0.1855%	19.89%
T2	0.3858%	0.3902%	1.84%
T3	0.0479%	$5.71 \cdot 10^{-4}\%$	$\sim \infty$
T4	0.0131%	$1.18 \cdot 10^{-4}\%$	$\sim \infty$

Table 5.2: Value of the percentage increase of the semi-major axis considering SRP only, SRP+PRP and the corresponding absolute percentage increase for a sail orbiting around the Earth.

These results can all be summarized in Table 5.2. The increases are function of the number of orbits the sail perform during the trajectory, while the absolute percentage increase is valid for any number of orbits. From these results it is possible to state that the consideration of the PRP enables to perform a semi-major axis increase manoeuvre even in the case with $\omega = 180$ and 270 deg, infeasible considering the SRP only. Moreover the PRP gives an additional contribution in every study-case considered in this work.

5.2 Venus

The same study has been conducted for a sail around Venus. In this case, since the high BBRP luminosity of the planet, the planetary radiation plays an important role in the results.

The study starts with an orbit with argument of peripasis $\omega = 0$ deg. Fig. 5.11 presents the trajectory and the corresponding orientation of the sail. When it is compared with the same case around the Earth (Fig. 5.2) a great difference can be found in the attitude angle of the sail in the arc. In this case, in fact, the sail faces the planet to gain the maximum acceleration. Considering Fig. 5.12a, in which the trend of the semi-major axis is plotted, it is easy to state that in this case the increment is greater than the case of a sail around the Earth. In fact the contribution of the PRP leads to a percentage increase of 889.9%. Moreover Fig.5.12b shows how the addition of the PRP enables the sail to experience acceleration seven times greater during the thrust. Fig. 5.12c shows how, close to the pericentre out of the arc, the minimum acceleration has a non-zero value due to the dominating contribution of the planetary radiation, as can be seen in the presence of the small peaks.

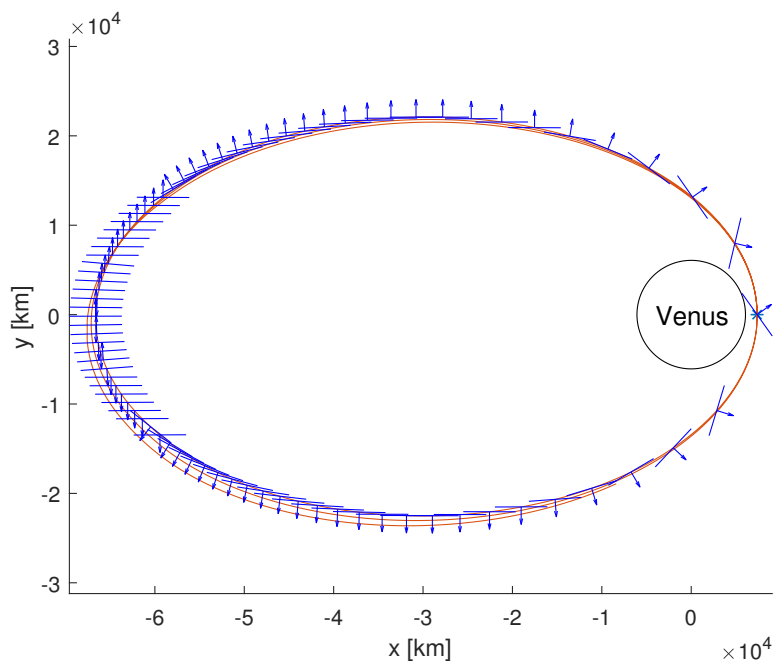
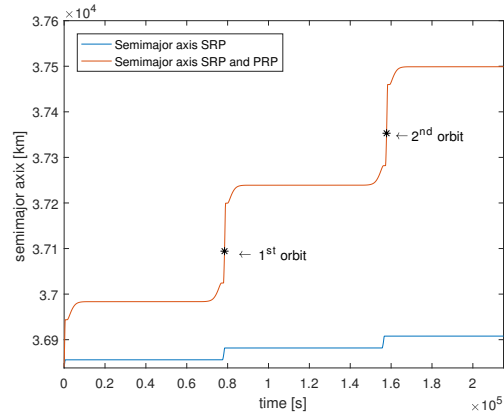
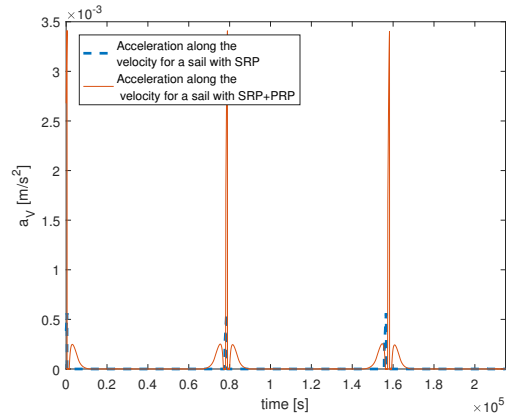


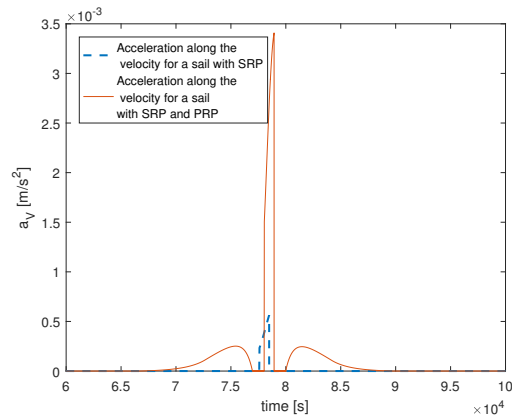
Figure 5.11: Trajectory around Venus with orientation of the sail with $\omega = 0$ deg



(a) Semimajor axis with SRP and SRP+PRP.



(b) Acceleration along the velocity for a sail with SRP and SRP+PRP.



(c) Acceleration along the velocity around the pericentre.

Figure 5.12: Results for a sail around Venus with $\omega = 0$ deg.

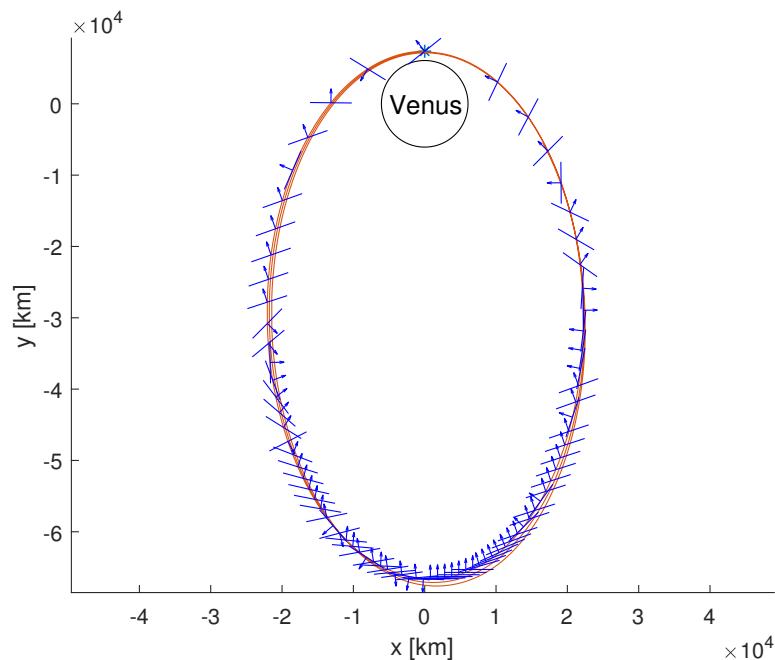
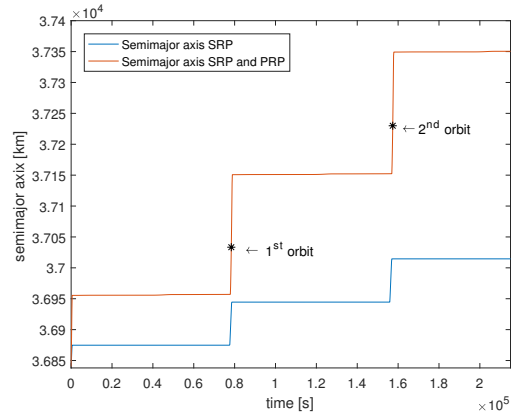
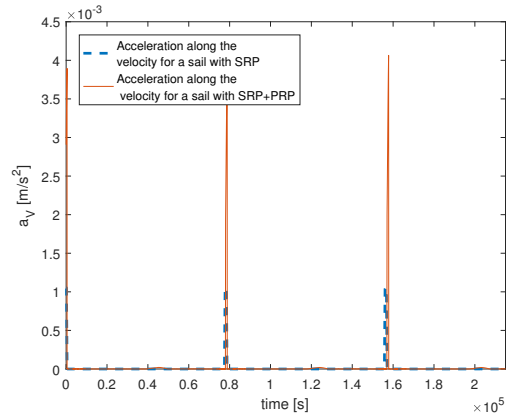


Figure 5.13: Trajectory around Venus with orientation of the sail with $\omega = 90$ deg

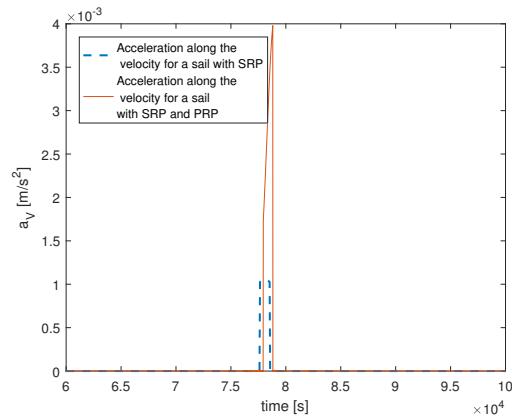
The following case presents a periapsis at $\omega = 90$ deg, for this case the results are shown in Fig. 5.14. As already explained, the sudden changes of attitude are caused by the numerical approach. The semi-major axis, for this starting orbit, has a percentage increase of 192.5%. This case presents the lowest contribution of the PRP since the position of the arc benefits from the positive contribution of the SRP. As regards the acceleration along the velocity direction, Figs. 5.14b and 5.14c shows how in this case the presence of the PRP leads to accelerations that are 4 times the one obtained in the case SRP only.



(a) Semimajor axis with SRP and SRP+PRP.



(b) Acceleration along the velocity for a sail with SRP and SRP+PRP.



(c) Acceleration along the velocity around the pericentre.

Figure 5.14: Results for a sail around Venus with $\omega = 90$ deg.

When the argument of periapsis has a value of $\omega = 180$ deg the sail orbits along the trajectory showed in Fig. 5.15 and it experiences an increase of the semi-major axis that is infinite. In fact, as can be seen in Fig. 5.16a, a stays almost constant when only the SRP is considered since the arc is in eclipse and the acceleration is null in every point of the trajectory (Fig. 5.16b). Adding the PRP enables the increase of the semi-major axis and leads to a non-zero acceleration in the arc, as can be seen Fig. 5.16b.

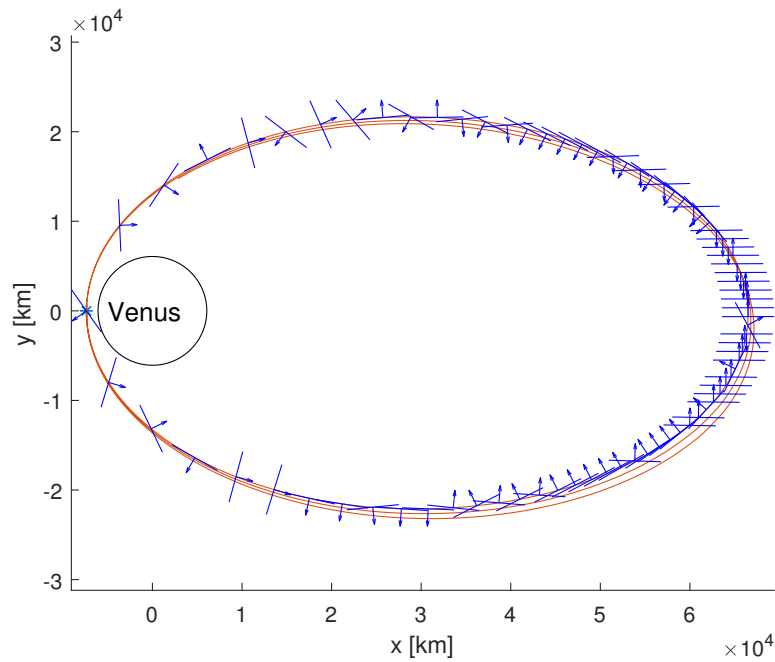
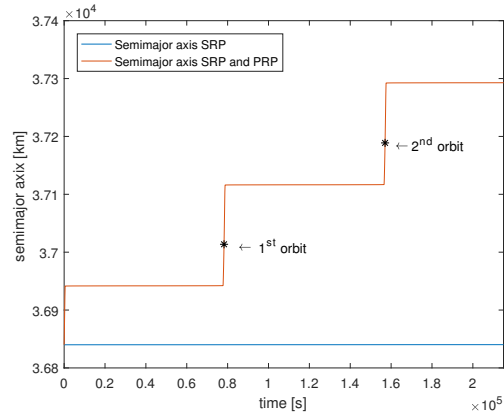
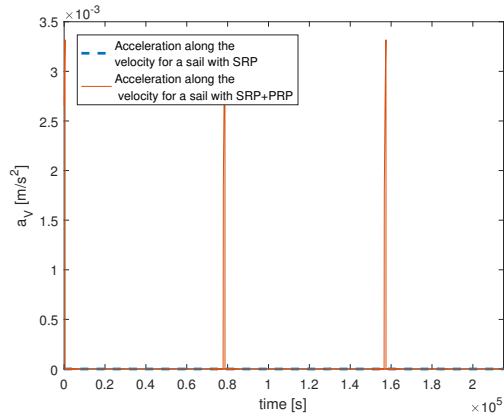


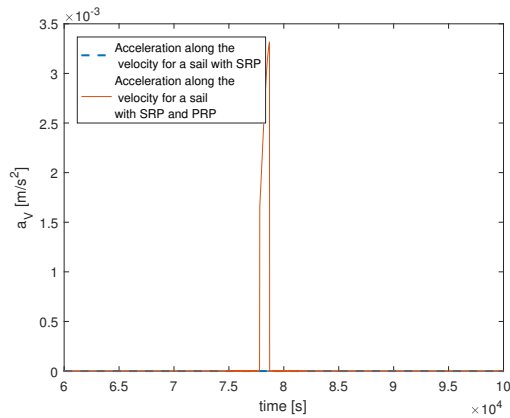
Figure 5.15: Trajectory around Venus with orientation of the sail with $\omega = 180$ deg



(a) Semimajor axis with SRP and SRP+PRP.



(b) Acceleration along the velocity for a sail with SRP and SRP+PRP.



(c) Acceleration along the velocity around the pericentre.

Figure 5.16: Results for a sail around Venus with $\omega = 180$ deg.

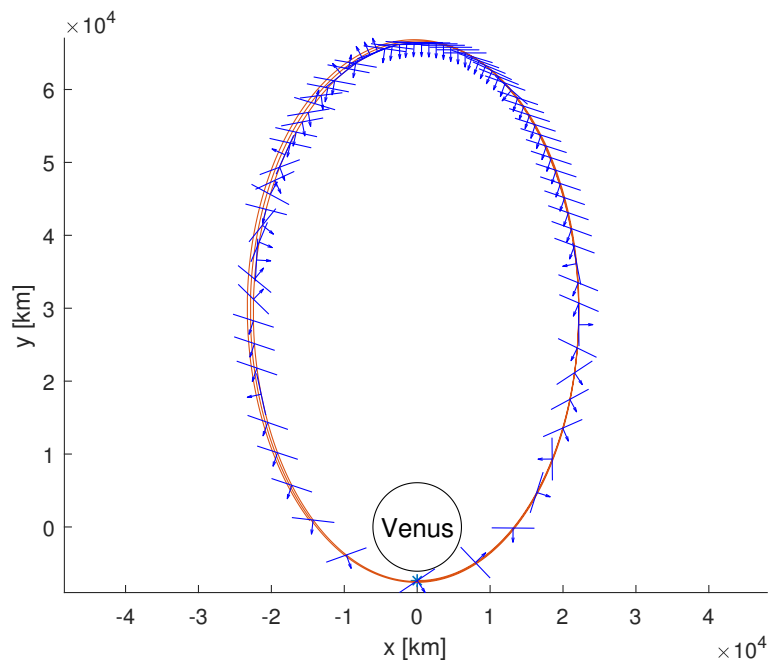
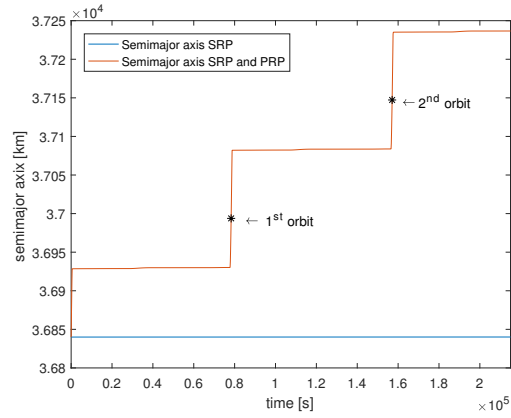
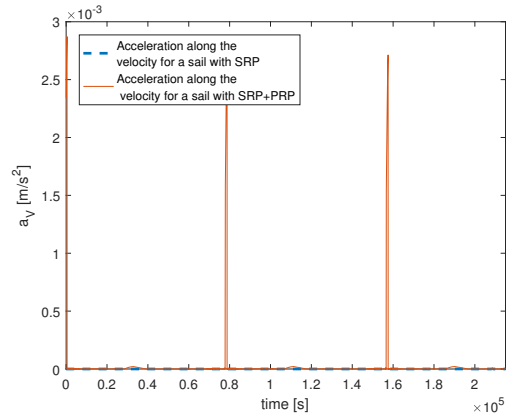


Figure 5.17: Trajectory around Venus with orientation of the sail with $\omega = 270$ deg

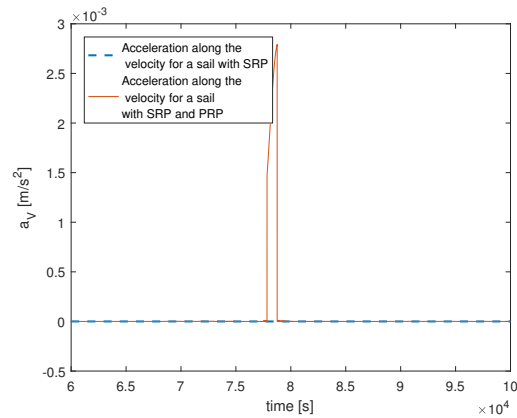
The last case studied is the one in which the periapsis is at $\omega = 270$ deg. In this case the position of the burn arc is subject to the negative contribution of the Sun. For this reason the case SRP only leads to a null increment of the semimajor axis, since the maximum acceleration of the sail is zero (Fig. 5.18a). Different results can be obtained considering the PRP, the radiation coming from the planet enables to increase a . This means that the percentage increment of the semi-major axis is infinite. As regards the acceleration, Fig. 5.18c shows how the PRP changes the trend, generating great accelerations during the thrusting arc. Also in this case, as already explained for the Earth, the sail thrusts a little bit also out of the arc. It can be deduced from the small peaks in Fig. 5.18b, but this phenomenon is smaller than in the case of a sail around the Earth. From Figs. 5.13, 5.15 and 5.17 it seems that the sail steers randomly, as already mentioned for the Earth, this behaviour is only the consequences of a numerical issue, since the minimum acceleration is found for different value of the attitude angle.



(a) Semimajor axis with SRP and SRP+PRP.



(b) Acceleration along the velocity for a sail with SRP and SRP+PRP.



(c) Acceleration along the velocity around the pericentre.

Figure 5.18: Results for a sail around Venus with $\omega = 270$ deg.

Table 5.3 summarises the results obtained in this section. Around Venus the beneficial contribution of the PRP is huge, with percentage increase over 100% for every value of ω . This means that the consideration of the PRP for a sail orbiting around Venus is fundamental, since it enables the sail to have much better performances.

Trajectory	Increase with SRP+PRP	Increase with SRP	Absolute percentage increase
T1	1.8431%	0.1862%	889.8%
T2	1.3862%	0.4738%	182.5%
T3	1.2296%	$6.8 \cdot 10^{-4}\%$	$\sim \infty$
T4	1.0772%	$2.13 \cdot 10^{-4}\%$	$\sim \infty$

Table 5.3: Value of the percentage increase of the semi-major axis considering SRP only, SRP+PRP and the corresponding absolute percentage increase for a sail orbiting around Venus.

Finally, in Table 5.4 are presented the values of the semi-major axis, eccentricity and argument of periapsis at the initial and final time of the trajectory around Earth and Venus for different starting ω .

Analysing these results helps to realise how the addition of the PRP generates much greater increments in the case of a sail orbiting around Venus. This is due to the fact that the luminosity of the planet is of almost two order of magnitude greater than the one obtained for the Earth. It is important to remember that this results corresponds to a time of three orbits, better results can be obtained integrating for a longer period. From these results it is possible to state that the PRP gives

Trajectory	Initial orbital elements			Earth			Venus		
	ω_i [rad]	a_i [km]	e_i	ω_f [rad]	a_f [km]	e_f	ω_f [rad]	a_f [km]	e_f
T1	0	36840	0	0.0023	36908	0.8003	0.0421	37519	0.8029
T2	1.5708	36840	0	1.5712	36984	0.8017	1.5919	37351	0.8121
T3	3.1416	36840	0	3.1409	36858	0.8001	3.0959	37293	0.8026
T4	4.7124	36840	0	4.7129	36845	0.87992	4.7347	37237	0.7929

Table 5.4: Orbital element at the initial and final time for different trajectories around Earth and Venus.

a beneficial contribution both around Earth and Venus. In particular around the latter planet the radiation coming from the Venus is the dominating contribution, generating acceleration much greater than the one obtained in the case SRP only. Moreover for both the study-cases the addition of PRP enables the increase of the semi-major axis also in cases infeasible considering solely the SRP.

Chapter 6

Conclusions

In this work, a solar sail orbiting around a planet was considered, investigating the contribution of the planetary radiation pressure to the acceleration of the sail. The effects of the solar and planetary radiation pressure were developed using opportune models that considered the optical characteristics of the sail, the directions of the incident radiations and, in the case of the planetary radiation, the presence of black-body radiation and albedo. This allowed the description of all possible orientations of the sail in a grid of points around the planet to maximise the acceleration along a given direction. Results in this case showed that if the sail is orbiting around the Earth, there is not a substantial difference with the case with solar radiation only. If the considered planet is Venus, results changed, with the radiation coming from the planet that becomes the dominating factor in the orientation of the sail. Moreover it has been found that the greatest contribution is given by the BBRP, especially around Venus, while the albedo has almost the same magnitude around both planets.

Using Gauss' equations, an increasing semi-major axis manoeuvre has been integrated, using a tangential control law around Earth and Venus. Planetary radiation has a contribution in the acceleration experienced by the sail. However in the case of a sail orbiting around the Earth this contribution is not much great, but still it can be considered as an additional factor to the force and it enables to performance semi-major axis increase also when $\omega = 180$ or 270 deg.

When a sail orbiting around Venus is considered, planetary radiation pressure is by far the dominating contribution, providing better performances of the sail, not only in the eclipse region, but everywhere close to the planet. The increase of the semi-major axis are over 100% for each position of the argument of periapsis, showing that not considering this contribution leads to worse performances of the planetary sail.

This was a preliminary study to investigate whether and how the inclusion of the radiation of the planet changes the behaviour of a sail. More accurate results could

be obtained improving the models used for the planetary radiation pressure force, for the albedo and for the eclipse. In this case the planet was considered as a uniformly bright disc. Since the vicinity of the sail to the planet, the consideration of the celestial body as a uniformly bright sphere emitting radial radiation could give results more consistent with reality. Moreover the albedo so far has been modelled using an engineering approach, this model could be improved considering the portion of the planetary sphere illuminated by the Sun and the amount of the reflected light that impact the surface of the planet. As regards the eclipse region, the cylindrical eclipse model could be replaced with one considering the divergence of the Sun light rays. Moreover since the energy coming from the planet is in the infra-red range, a study regards the material of the sail should be conducted, to analyse how the sail reflects radiation in this energy range.

To simplify the problem, a two dimensional study-case have been considered, however the application of a three dimensional model could lead to results that consider also the out of plane variations and the assumption of a fixed Sun could be relaxed, showing a real scenario.

The results obtained in this study could be used for future works. When a mission in the vicinity of Venus is considered, the presence of the planetary radiation should be taken into account, since the performance of the sail improved a lot. Moreover, both around Venus and Earth, the presence of the planetary radiation is important in the eclipse region.

Future studies can consider the combined effect of solar and planetary radiation pressure together with the effect of the aerodynamic forces. If a sail orbiting in the atmosphere of the planet is taken into account, interesting results can be obtained. In this scenario the sail is closer to the planet, experiencing also a greater planetary radiation.

Further analysis could also be conducted on the optimisation of the control law, studying how it changes whether the PRP is considered or not.

Appendix A

Electromagnetic description

Another way to explain this phenomenon is using the electromagnetic description of light [1]. In this case the momentum is transported to the solar sail by electromagnetic waves. \mathbf{E} is the electric field component of the wave, it induces a current \mathbf{j} in the sail. The magnetic component of the incident wave \mathbf{B} generates a Lorentz force equal to $\mathbf{j} \times \mathbf{B}$ along the direction of propagation of the wave. Another electromagnetic wave, observed as a reflection wave, is generated by the induced current \mathbf{j} . Taking into account a wave propagating along the x -axis, it is possible to express the force exerted on a current element as

$$df = j_z B_y dx dy dz \quad (\text{A.1})$$

where j_z is the current density induced in the surface of the reflector. The pressure can be defined as the force per unit area

$$dP = j_z B_y dx \quad (\text{A.2})$$

Recalling the Maxwell's equations of electrodynamics it is possible to express the term in Eq. A.2 with a field term. The time average pressure is then give by

$$\langle dP \rangle = -\frac{\partial}{\partial x} \left(\frac{1}{2} \epsilon_0 E_z^2 + \frac{1}{2\mu_0} B_y^2 \right) dx \quad (\text{A.3})$$

Where ϵ_0 is the permittivity of free space and μ_0 is the permeability of free space. In parentheses is possible to identify the energy density U for the electric component E and magnetic component B of the incident wave

$$U = \frac{1}{2} \epsilon_0 E^2 + \frac{1}{2\mu_0} B^2 \quad (\text{A.4})$$

Integrating Eq. A.3, it is possible to obtain the pressure exerted on a surface of thickness Δl

$$\langle P \rangle = - \int_0^{\Delta l} \frac{\partial U}{\partial x} dx \quad (\text{A.5})$$

The pressure exerted on the surface is equal the total energy density if the medium is a perfect reflector.

Two plane waves, separated by a distance Δx , are considered. Both of them are incident on a surface of area A . It is possible to express the distance Δx as $\Delta x = c\Delta t$, where Δt is the travel time between the wave fronts. Moreover the volume of space between the two waves is $A\Delta x$. Hence the energy density can be written as

$$U = \frac{\Delta E}{A(c\Delta t)} \quad (\text{A.6})$$

The energy flux W across the surface is given by

$$W = \frac{1}{A} \left(\frac{\Delta E}{\Delta t} \right) \quad (\text{A.7})$$

Recalling the expression in Eq. A.6, it is possible to express the energy density as

$$U = \frac{W}{c} \quad (\text{A.8})$$

Comparing Eqs. A.8 and 2.13 it is possible to assert that both the descriptions, quantum and electromagnetic, lead to the same result.

Bibliography

- [1] C. R. McInnes, *Solar Sailing Technology, Dynamics and Mission Applications* Chichester, UK, Springer, 1999.
- [2] V. J. Lappas, S. Leipold, P. Falkner, “Attitude Design for Solar Sail Missions” in *6th International ESA Conference on Guidance, Navigation and Control Systems, European Space Agency, Loutraki, Greece, 2005*, pp. 191–194.
- [3] L. Johnson, M. Whorton, A. Heaton, R. Pinson, G. Laue, C. Adams, “NanoSail-D: A solar sail demonstration mission” in *Acta Astronautica*, v. 69, pp. 571–575, 2011.
- [4] V. J. Lappas, N. Adeli, L. Visagie, J. Fernandez, T. Theodorou, W. Steyn, M. Perren, “CubeSail: A low cost CubeSat based solar sail demonstration mission” in *Advances in Space Research*, v. 48, pp. 1890–1901, 2011.
- [5] S. Eguchi, N. Ishii, H. Matsuo, “Guidance strategies for solar sail to the Moon” in *AAS 93-653. Advances in Astronautical Science*, v. 85, pp. 1419–1433, 1993.
- [6] T. A. Fekete, L. Sackett, A. H. von Flotow, “Trajectory design for solar sailing from low-Earth orbit to the Moon” in *AAS 92-184. Advances in Astronautical Science*, v. 79, pp. 1083–1094, 1992.
- [7] C. E. Garner, H. Prince, D. Edwards, Baggett, “Developments and activities in solar sail propulsion” in *AIAA-2001-3234, 37th AIAA/ASME/SAE/ASEE Joint Propulsion Conference*, Salt Lake City, UT, USA, July 2001.
- [8] M. Leipold, “Solar Sail Mission Design. Doctoral Thesis. Lehrstuhl für Flugmechanik und Flugregelung” in *Technische Universität München*, v. DLR-FB-2000-22, 1999.
- [9] R. Frisbee, J. Brophy, “Inflatable solar sail for low-cost robotic Mars missions” in *33rd Joint Propulsion Conference and Exhibit, Joint Propulsion Conferences*, 1997.
- [10] G. Colasurdo, L. Casalino, “Optimal control law for interplanetary trajectories with solar sail” in *Advances in the Astronautical science*, v. 109 (3), pp. 2357–2368, 2001.
- [11] M. Malcolm, M. Colin, “Solar sail science mission applications and advancement” in *Advances in Space Research*, v. 48, 2011.
- [12] M. Malcolm, H. Gareth, M. Colin, L. Aleksander, F. Peter, A. Alessandro,

- “GeoSail: An Elegant Solar Sail Demonstration Mission” in *Journal of Spacecraft and Rockets*, v. 44.
- [13] M. Leipold, W. Seboldt, S. Lingner, E. Borg, A. Herrman, A. Pabsh, O. Wagner, J. Bruckner, “Mercury Sun-synchronous polar orbiter with solar sail” in *Acta Astronautica*, v. 39.
- [14] V. L. Coverstone, J. E. Prussing, “Technique for escape from Geosynchronous Transfer Orbit using a solar sail” in *Journal of Guidance, Control, and Dynamics*, v. 26, July-August.
- [15] J. W. Hartmann, “Escape from Earth using a solar sail” in *Dep. of Aeronautical and Astronautical Engineering, Final Rept. for AAE 493 Independent Study, Univ. of Illinois, Urbana-Champaign*.
- [16] M. Macdonald, C. R. McInnes, “Realistic Earth Escape Strategies for Solar Sailing” in *Journal of Guidance, Control, and Dynamics*, v. 28.
- [17] V. Stolbunov, M. Ceriotti, C. Colombo, C. R. McInnes, “Optimal law for inclination change in atmosphere through solar sailing” in *Journal of Guidance, Control, and Dynamics*, v. 36.
- [18] G. Mengali, A. A. Quarta, “Near-Optimal Solar Sail Orbit-Raising from Low Earth Orbit” in *Journal of spacecraft and rockets*, v. 42.
- [19] M. E. Grottee, M. J. Holzinger, “Solar sail equilibria with albedo radiation pressure in the circular restricted three-body problem” in *Advances in Space Research*, v. 59, 2017.
- [20] in “Resolution B3 on recommended nominal convention constants for selected solar and planetary properties” 2015. Retrieved 5 June 2018.
- [21] T. S. Kuhn, “Black-Body Theory and the Quantum Discontinuity” in *Oxford University Press*.
- [22] J. Stefan, in “Über die Beziehung zwischen der Wärmesthaltung und der Temperatur” 1879.
- [23] E. A. Thornton, in “Orbiting space structures” 1996.
- [24] R. H. Battin, *An introduction to the Mathematics and Methods of Astrodynamics* New York, rev. ed., AIAA Education Series, AIAA, 1999, pp.488-489.
- [25] Y. Gao, in “Near-optimal very low-thrust Earth-orbit transfers and guidance schemes” v. 30.